

Cyclooxygenase-2 plays a crucial role during myocardial patterning of developing chick

BHAVAL K. PARMAR, URJA R. VERMA, JUHI A. VAISHNAV, SURESH BALAKRISHNAN*

Department of Zoology, Faculty of Science, The Maharaja Sayajirao University of Baroda Gujarat, India

ABSTRACT Cyclooxygenase-2 (COX-2), a member of the Cyclooxygenase family, initiates the biosynthesis of prostanoids that regulates various cellular functions. Our pilot attempt revealed that the administration of etoricoxib, an inhibitor specific for COX-2, induces abnormal looping in the chicken heart. The present study attempts to reveal the mechanistic details of etoricoxib-induced abnormal cardiac looping. The activity of COX-2 was inhibited by administering 3.5 µg of etoricoxib into the egg's air cell on day zero of incubation. The gene and protein expression patterns of key mediators of heart development were then analyzed on day 2 (HH12) and day 3 (HH20). Reduced COX-2 activity altered the expressions of upstream regulators of organogenesis like Wnt11, BMP4, and SHH in the etoricoxib-exposed embryos. The observed expression shifts in the downstream regulators of myocardial patterning (MYOCD, HAND2, GATA4, GATA5, and GATA6) in the treated embryos corroborate the above results. In addition, the reduction in COX-2 activity hampered cardiomyocyte proliferation with a concomitant increase in the apoptosis rate. In conclusion, the collective effect of altered expression of signaling molecules of myocardial patterning and compromised cardiomyocyte turnover rate could be the reason behind the looping defects observed in the heart of etoricoxib-treated chick embryos.

KEYWORDS: chick embryo, heart development, cyclooxygenase-2, looping, trabeculation

Introduction

Congenital malformations are observed in at least 1% of newborn babies and conotruncal heart defects pose the highest in-utero mortality risks (Lutin *et al.*, 1999; Dees *et al.*, 2000). There is ample evidence suggesting that mortality remains high even after postnatal surgical repair (Khoshnood *et al.*, 2012), making it imperative to understand the genesis of these defects.

Research on heart development has witnessed a renaissance in recent years. We still do not understand the defects' correlation with the looping, convergence, and wedging process. As the segments of the cardiac tube are in sequence and are not separated, looping creates an inflow and an outflow tract (proximal and distal tract) (Van den Hoff *et al.*, 1999). Both inflow and outflow tracts are brought together cranio-caudally through convergence (Yelbuz *et al.*, 2002). After the tract has converged, the inflow portion of the tube nestles behind the ventrally placed outflow tract, beginning a new period of outflow tract adjustment called wedging (Bartelings and Gittenberger-de, 1989). These processes occur in heart tubes and develop into a four-chambered heart in aves and mammals. In aves, the heart tube development starts at day one, and due to

external development, looping patterns are evident in chick embryos of day 2 and day 3. Further, the molecular signaling was also reported to be similar in the case of aves and mammals, making the chick embryo an excellent model to study heart development (Olson, 2006).

Convergence and wedging of the heart tube require multiple cellular events such as cell proliferation, migration, and differentiation governed by molecules such as Wnts, BMPs, GATAs, and Shh. The expression of zinc finger transcription factors (GATA4, GATA5, and GATA6), which are known to regulate cell differentiation and cell number in the heart field, has been reported to be conserved throughout the vertebrate lineage (Nemer, 2008; Van Berlo and Maillet, 2010). During the initiation of the heart tube, myocardin

Abbreviations used in this paper: COX, Cyclooxygenase; BMP, Bone morphogenetic protein; HAND, Heart and Neural Crest Derivatives Expressed; PGE2, Prostaglandin E2; TGF-β, Transforming growth factor-β; HH, Hamburger and Hamilton stages; MyoCD, Myocardin; DAPI, 4',6-diamidino-2-phenylindole; PCNA, Proliferating cell nuclear antigen; GAPDH, glyceraldehyde-3-phosphate dehydrogenase; SHH, sonic hedgehog; TBX, T-Box Transcription Factor; ANF, Atrial natriuretic factor.

*Address correspondence to: Suresh Balakrishnan, Department of Zoology, Faculty of Science, The Maharaja Sayajirao University of Baroda Gujarat, 390 002, India. E-mail: b.suresh-zoo@msubaroda.ac.in - https://orcid.org/0000-0002-6559-022X

Submitted: 21 November, 2022; Accepted: 22 December, 2022; Published online: 22 December, 2022.

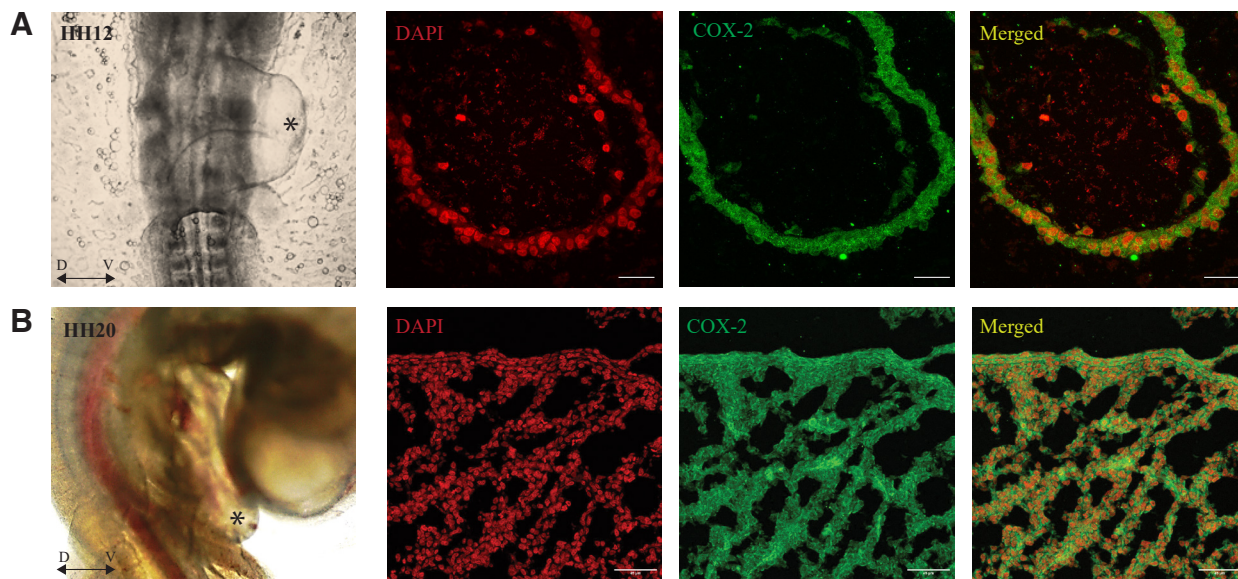


Fig. 1. Immunolocalization of COX-2 in the developing heart of control embryos. (A) HH12 (day 2) control embryo (ventral side) shows COX-2 localization in the cytoplasm of a single layer of cardiomyocytes of the developing heart tube. The black asterisk indicates the section plane of the heart region. (B) HH20 (day 3) control embryo (ventral side) shows COX-2 protein expression in the cytoplasm of cells on the outer wall of the heart; also, the trabecula shows the presence of COX-2. The black asterisk shows the plane of section of the heart region, D ↔ V: represent Dorsal-Ventral orientation.

expresses in the cells destined to become cardiac muscle (Chen *et al.*, 2008). Moreover, HAND2 guides the migrating cells of the heart to achieve symmetry during the looping process (Laurent *et al.*, 2017). Studies suggested that T-box transcription factors (TBX) interact with GATA genes, which coherently help sculpt vertebrates' hearts (Stennard *et al.*, 2003). GATA5 assists in regular cardiomyocyte migration, especially during ventricular wall compaction. Trabeculation defects and valvular dysfunction have been identified as consequences of deviated GATA5 expression in chick embryos (Pérez-Pomares and Pompa, 2011).

Among the variety of regulatory factors regulating cardiac tube looping and cardiac patterning, a key molecule is COX-2, an inducible isoform of cyclooxygenase that catalyzes the formation of

PGE₂ from arachidonic acid (Ricciotti and FitzGerald, 2011). COX-2 mediated PGE₂ synthesis plays a crucial role in cellular events such as proliferation, migration, and differentiation by modulating the regulators of signaling pathways such as Wnt/ β -catenin, BMP, and TGF- β (Neil *et al.*, 2008; Jana *et al.*, 2016; Buch *et al.*, 2017). A study by Xu and coworkers showed that COX-2 inhibition using celecoxib causes defective heart formation and hinders the looping of heart tubes in zebrafish embryos (Xu *et al.*, 2011).

A previous study from our laboratory showed that COX-2 inhibition by etoricoxib causes defects in limb development, vascularization, tissue integrity, and organ patterning in developing chicks, where the most lethal malformation was found in the heart region (Verma *et al.*, 2021). This study observed that selective COX-2 inhibition reduces levels of PGE₂ while the remaining prostanoids maintain their average titer. Based on these findings and other reported interactions of COX-2 with different signaling molecules, we hypothesize that the pathways regulating heart tube looping and chamber formation might be affected due to COX-2 inhibition, resulting in developmental heart defects in embryos.

In order to validate this notion, the present study inhibited COX-2 activity using etoricoxib, a selective COX-2 inhibitor, and its effects on the regulators of heart tube looping and chamber formation were ascertained in day 2 and day 3 chick embryos.

Results

Defective looping of heart tube on HH12 (day 2)

Immunolocalization indicates that COX-2 is located in the cytoplasmic region of the heart tube cells (Fig. 1A).

COX-2 activity was recorded in control and etoricoxib-treated embryos. There was a significant decrease in the COX-2 activity on day 2 of the developing embryo (Fig. 2, Table S1).

On day 2 (HH 12), the control group embryo showed a typical

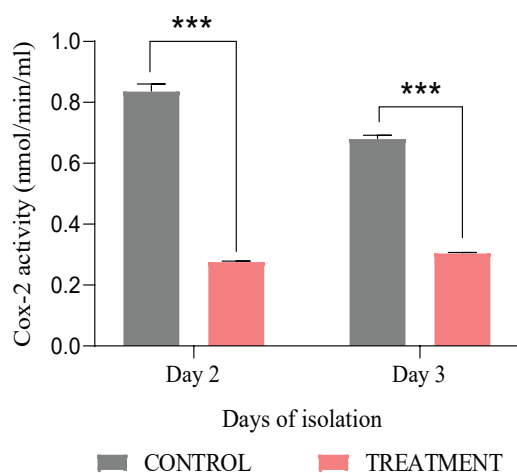


Fig. 2. COX-2 assay for day two and day three embryos. Enzyme activity is expressed as Mean \pm SEM, n=3, with 30 eggs per group per day. ***p \leq 0.001.

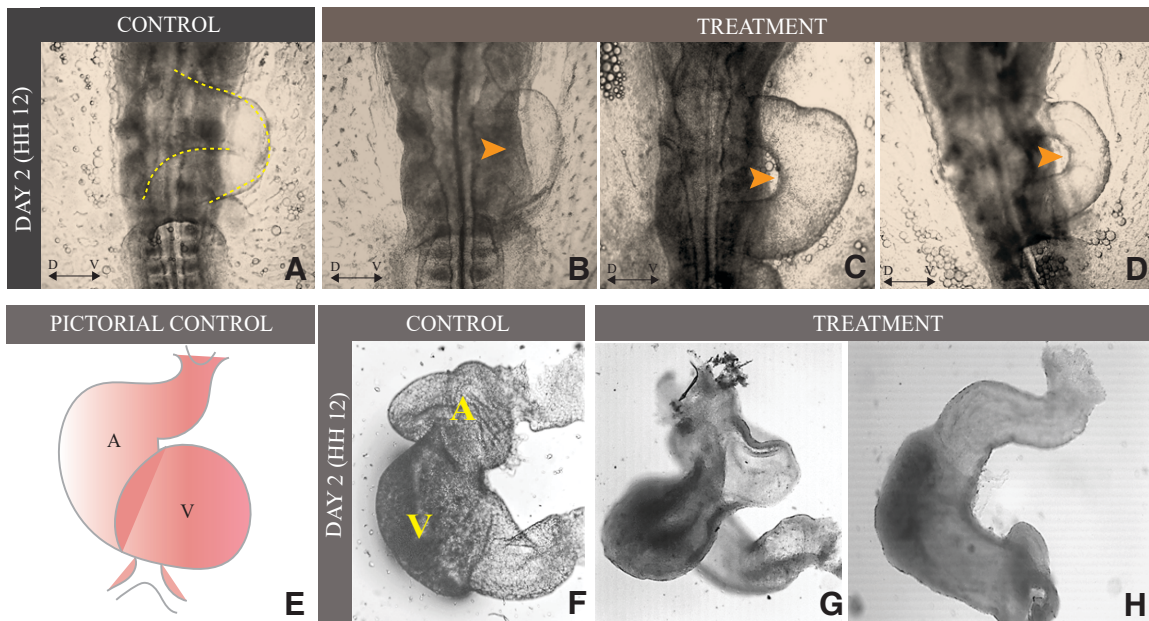


Fig. 3. Etoricoxib exposure causes abnormal heart tube looping in the embryo on day 2. (A) Normal looping of the heart tube found in the control group of the embryo on the ventral side (the dotted line represents normal looping of the heart). (B-D) Abnormal looping of heart tube in etoricoxib-treated embryos represented by orange arrowheads. (E) Pictorial representation of day two heart of control embryo. (F) Isolated heart of control embryo. (G-H) Abnormal looping in isolated heart tube and uneven thickening of the tube. A: Auricle, V: Ventricle, D ↔ V: represent Dorsal-Ventral orientation.

S-shaped heart tube (Fig. 3A). In contrast, the embryos from the treatment group showed obvious signs of defective heart looping. In addition, the rate of heart tube loop malformations was significantly high in the treated embryos. Aberrations, such as underdeveloped heart, distorted heart tube, and defective heart tube curvature, were frequently observed in etoricoxib-treated embryos (Fig. 3B-D). A visual comparison of heart tissues isolated from the control and treatment group of day 2 embryos suggests heart-loop defect (Fig. 3F-H).

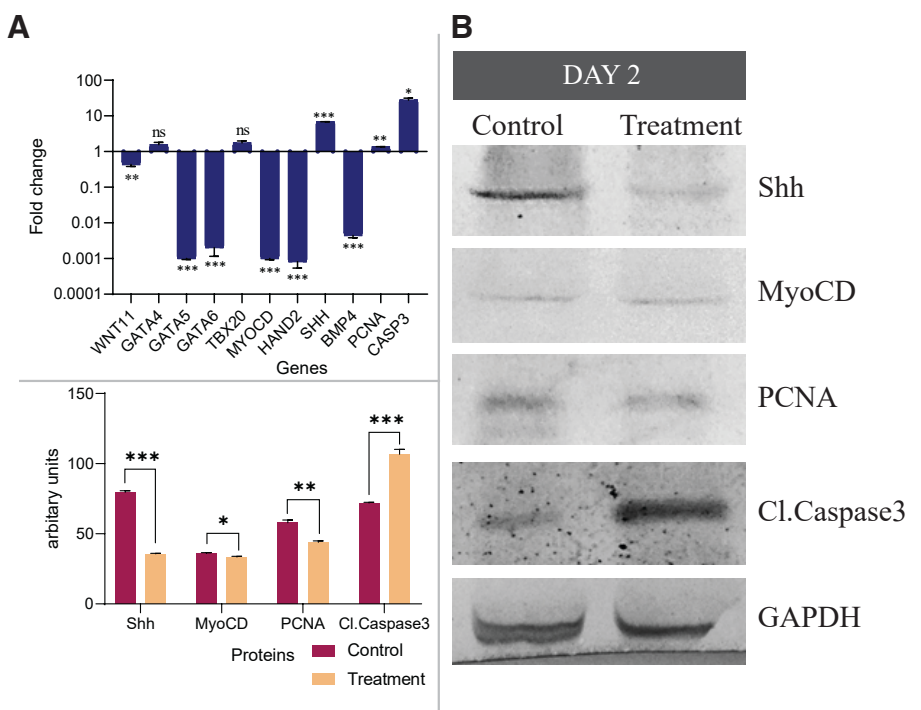
Studies involving gene expression were carried out to determine heart-loop deviation. The mRNA levels of genes that play a significant role in heart tube patterning and looping, viz. WNT11, GATA5, GATA6, and BMP4 were significantly reduced in the etoricoxib-treated embryos (Fig. 4A). However, the transcript levels of genes involved in the looping and maturation of the cardiomyocytes showed an aberrant expression pattern under the ablation of COX-2 activity. SHH, PCNA, GATA4, TBX20, and CASP3 mRNA levels increased,

while those of HAND2 decreased in the treated embryo group compared to control embryos. Relative mRNA expression levels of the cardiomyocyte-specific gene, namely MYOCD, also showed a significant reduction under the etoricoxib treatment (Fig. 4A, Table S2).

Concomitant immunoblot analysis for protein revealed reduced Shh, MyoCD, PCNA, and Cl.Caspase3 levels in treated embryos on day 2 compared to control embryos (Fig. 4 B,C, Table S4).

Fig. 4. Expression pattern of genes and protein regulating the looping of heart tube of day two embryos.

(A) mRNA levels of various genes of cardiogenesis. Fold changes are expressed as Mean±SEM. Fold change values for the control embryo is 1.0 for all the genes, n=3 with 30 eggs per group per day; *p<0.05; **p<0.01; ***p<0.001. (B) Quantification of western blots by densitometry. Relative band intensities were normalized to the intensity of GAPDH of the respective sample; *p<0.05; **p<0.01; ***p<0.001. (C) Protein levels of Shh, MyoCD, PCNA, and Cl.Caspase3. GAPDH was taken as a loading control.



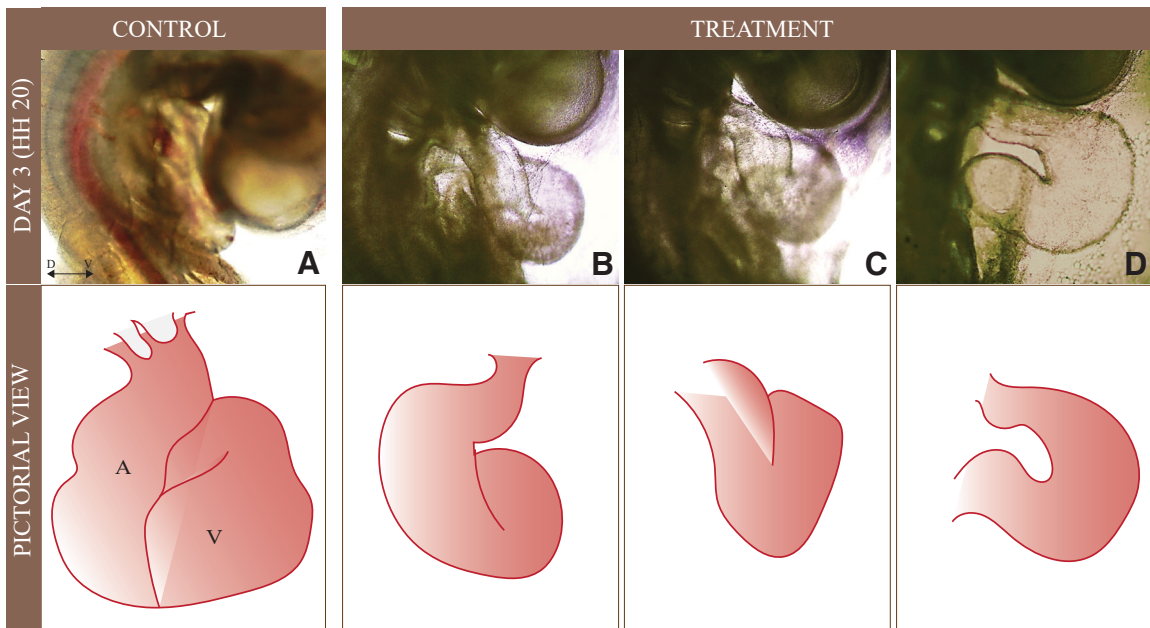


Fig. 5. Abnormal heart tube thickening and differentiation of chambers in the day three embryo. (A) Control embryo has thickening at ventricle walls, (B-D) Treatment group of the embryo has delayed development of the heart tube and uneven thickening of ventricular walls; the lower panel shows a pictorial representation of day three heart for normally developing embryo and under the exposure of etoricoxib. A: Auricle, V: Ventricle, D ↔ V: represent Dorsal-Ventral orientation.

Aberration in heart chamber formation on HH 20 (day 3)

Immunolocalization of COX-2 showed its expression in a normally developed day three embryo. The expression of COX-2 was found in the inner wall of the developing heart tube and in the trabeculae region (Fig. 1B).

Embryos from the day three treated group (HH 20) showed a significant decrease in COX-2 activity (Fig. 2) accompanied by a high rate of heart abnormalities. The control group displayed normal development and achieved the characteristic conical shape with heart tubes differentiated into auricles and ventricles (Fig. 5A). In contrast, the treated embryos showed many defects, including abnormal bending of the heart tube and straight heart tube. Moreover, the heart chambers, atria, and ventricles are not fully formed in treated embryos compared to control embryos (Fig. 5 B,D). Key signaling molecules involved in heart patterning and functioning were investigated at transcript and protein levels to corroborate the findings. In day

three treated embryos, relative mRNA expression levels exhibited remarkable downregulation of WNT11, GATA4, GATA6, TBX20, and BMP4. Likewise, the PCNA, SHH, and HAND2 transcript levels were conspicuously reduced in treated embryos (Fig. 6A, Table S3).

On the contrary, q-RT PCR analysis of GATA5, MYOCD, and CASP3 transcripts revealed an appreciable increase in their expression levels. To further substantiate the data at the transcript level, a Western blot was performed for key proteins responsible for cardiac patterning and loop formation. Densitometry analysis

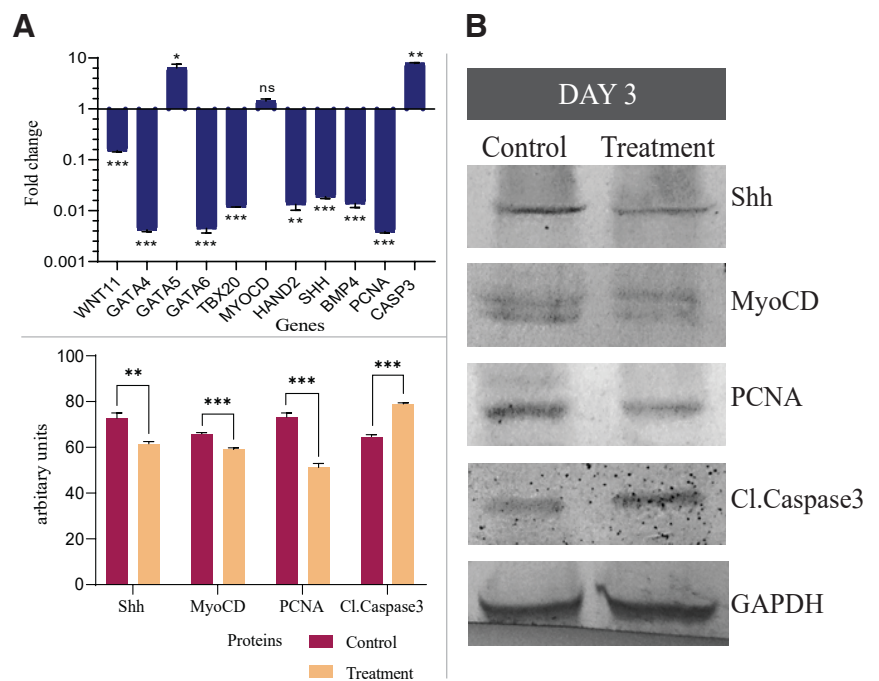


Fig. 6. Expression pattern of genes and protein regulating the heart tube thickening and chamber formation in day three embryos. (A) mRNA levels of various genes of cardiogenesis. Fold changes are expressed as Mean±SEM. Fold change values for the control embryo is 1.0 for all the genes, n=3 with 30 eggs per group per day; ns-non significant; *p≤0.05; **p≤0.01; ***p≤0.001. (B) Spot densitometry of western blot. Relative band intensities were normalized to the intensity of GAPDH of the respective sample; ns-non significant; *p≤0.05; **p≤0.01; ***p≤0.001. (C) Protein levels of Shh, MyoCD, PCNA and Cl.Caspase3. GAPDH was taken as a loading control.

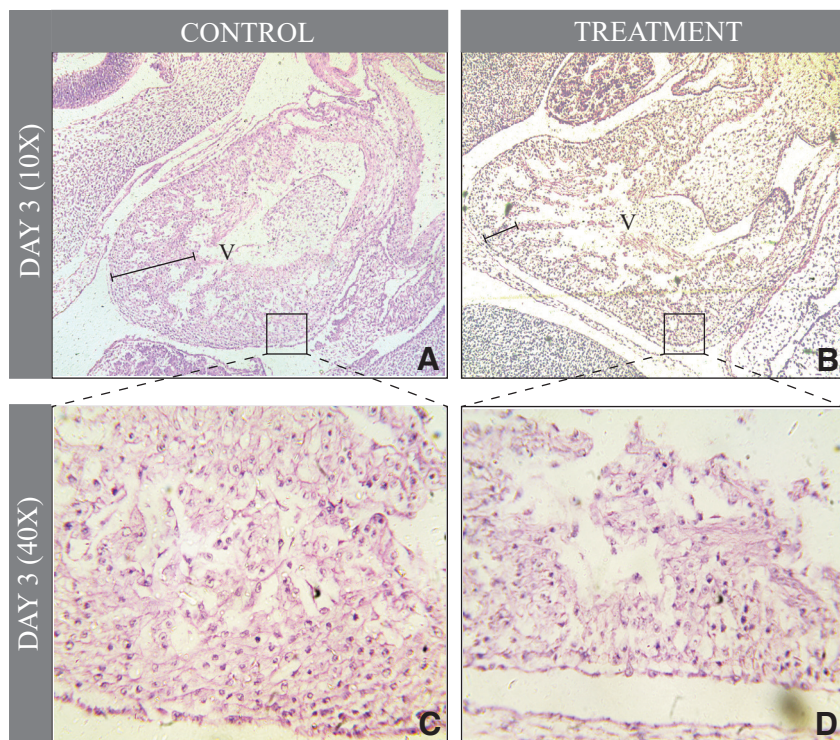


Fig. 7. Histology of day three heart. (A) Control heart (10X) has a triangular shape and dense ventricular walls at lower resolution (shown by the black line segment). (B) Etoricoxib treated heart have thin ventricular walls visible at 10x resolution (shown by the black line segment). (C) Inset image of control heart showing tightly packed cardiomyocytes showing normal trabeculation in the control group, magnification 40x. (D) Inset image of treatment group heart shows lack of cardiomyocytes packing in the ventricular wall. The loose arrangement of cells in the treated-embryonic heart confirmed the defect of trabeculation at the same stage as compared to the control group.

of Shh, MyoCD, and PCNA blots showed their levels significantly reduced under etoricoxib treatment. In contrast, Cl.Caspase3, an apoptotic marker, has exceptionally high expression levels in the embryos of the treatment group (Fig. 6 B,C, Table S4).

Additionally, the extent of heart patterning defects in HH 20 embryos was analyzed histologically. Control embryos revealed a functionally competent ventricular wall with standard compaction and trabeculation (Fig. 7 A,C). In opposition, the treatment group showed clear signs of ventricular non-compaction and defective trabeculation (Fig. 7 B,D).

Discussion

Many studies in mammals and other animal models have shown that COX-2-derived PGE₂ is an essential mediator of various physiological and pathological processes (Bondesen *et al.*, 2006; Pakrasi and Jain, 2008; Nørregaard *et al.*, 2015). Although studies have previously implicated the possible association of COX-2-derived PGE₂ with an embryonic malformation (Randall *et al.*, 1991), its role in the development of the heart or organogenesis of an embryo is still unknown. In this study, we hypothesized that aberrant COX-2 expression might interfere with embryological development during a critical period of embryogenesis, especially in heart development. Indeed, the COX-2 single knockout mice fetus exhibited severe

defects in the axial skeleton and died shortly after birth due to respiratory distress (Shim *et al.*, 2010). In a typically developing embryo, COX-2 expression is present to guide organogenesis, which was depicted by the immunolocalization method that clearly marked its contribution in the developing heart tube as well as walls of trabeculae on day 3.

The present study showed that when COX-2 activity has hampered, apoptosis in developing heart tubes dramatically increases, and the number of cardiomyocytes decreases. Additionally, trabeculae formation and cardiomyocytes condensation are impaired, leading to erroneous heart chamber formation under inhibition of COX-2 activity.

The Wnt signaling, both canonical and non-canonical, primarily regulates the heart tube's initial patterning, which plays an important role in deciding the fate of cardiomyocytes (Pandur *et al.*, 2002; Piven and Winata, 2017). In an isolated study, in a quail embryo, the dominant-negative Wnt11 construct decreased the expression of cardiac markers, hence not allowing cells to differentiate into cardiomyocytes in quail embryo. The expression of Wnt11 is found at a very early stage when paraxial plate mesoderm differentiates in developing chick embryos (Eisenberg and Eisenberg, 1999). We observed a significant decrease in Wnt11 level in the heart-forming tissues of day two and three chick embryos subjected to the selective inhibitor of COX-2 (etoricoxib). Due to the decrease in Wnt11 levels in the treatment group of embryos, the downstream molecules, such as GATA family members, showed deviated expression patterns.

Furthermore, specific genes and proteins were analyzed to understand the molecular aspects of the defects mentioned above. GATA5 is one such transcription factor that regulates myocyte number during heart development. GATA5 decrease in day two embryos hampers the cardiomyocyte formation, while on day three, it increases, which can be an outcome of a feedback loop. Its role in migration during early embryogenesis is also known (Peterkin *et al.*, 2007). Deviant expression of GATA5 was reported to induce trabeculation defects, valvular dysfunction, epicardia, and mesenchymal malformation in chick embryos (Chen and Fishman, 2000; Laforest *et al.*, 2011). Our findings also revealed a similar trend in expressing GATA5 and the anatomical features in the day two and day three embryos. We found deformed trabeculae in the treated group heart on day 3. Based on the results highlighted above, it is prudent to presume that COX-2 inhibition modulates the expression of GATA5.

Another transcription factor that facilitates the migration of cardiomyocytes is GATA4. It is reported that GATA4 expresses during the early stages of heart development, from the migration of pre-cardiac cells to the complete heart tube formation (Lopez-Sanchez *et al.*, 2009). It has been observed that in homozygous GATA4 null mice, the erroneous migration of pro-myocardial primordia resulted in two independent heart tubes (Molkentin *et al.*, 1997). The experimental group of embryos showed impaired expression of GATA4 compared to the control embryos. The data shows that GATA4 increased on day two and then decreased on day three embryos under the etoricoxib treatment. Reports suggest

that GATA4 and GATA5 genes cooperatively in zebrafish perform functions such as liver and heart organogenesis and myocyte population regulation. (Singh *et al.*, 2010). There is ample evidence suggesting that the other GATA gene compensates for each GATA gene's expression if one gene goes downregulated (Laforest and Nemer., 2011). The antagonistic expression pattern observed for GATA4 and GATA5 for day two and day three treated embryos agrees with the above notion.

Recent studies demonstrated that conditional deletion of GATA6 leads to malformation of the cardiac outflow tract and aortic arch arteries (Lepore *et al.*, 2006). In our studies, the level of the GATA6 transcription factor decreased on day two and day three under the treatment of etoricoxib. The declined levels of GATA6 led to defective outflow track formation in the day three embryo, which was visible in histology. Moreover, it has been suggested that increased levels of GATA6 may compensate for the loss of GATA4 in chicks (Narita *et al.*, 1997). Similar results were also found in our studies on day three embryos when treated with etoricoxib.

In addition, a vital molecule responsible for cardiac morphogenesis is the T-box transcription factor (TBX). The TBX family members interact with GATA factors and, together, contribute to sculpting the heart in vertebrates. According to a report, when TBX20 mutates, heart development is seized at the tube stage with no further development (Plageman and Yutzey, 2004). Moreover, it has been reported that TBX20 co-express with GATA5 and regulates myocyte population (Laforest and Nemer, 2011). The morphological observations of day two embryos of the treatment group revealed looping defects in the heart tube. The transcript level analysis of TBX20 and GATA5 revealed an antagonistic expression pattern (heightened expression of TBX20 with a concomitant reduction in GATA5). It is well known that TBX20 acts as a transcriptional regulator of the ANF (atrial natriuretic factor). However, the promoter region of the ANF is responsive to other factors, one of which is TBX5.

Nevertheless, when TBX5 acts as an activator, TBX20 acts as a repressor for ANF (Plageman and Yutzey, 2004). This intricate relationship between T-box transcriptional factors and downstream genes allows the formation of inflow and outflow tracks, atrioventricular cushions and valves at different time points during cardiac morphogenesis (Brown *et al.*, 2005). The lowered levels of TBX20 could hinder the standard sculpting of the heart in developing embryos despite having high levels of GATA5 under the etoricoxib treatment on day 3.

Moreover, the MYOCD gene that directs the myocardin protein synthesis expresses in an early embryo's heart field (Huang *et al.*, 2009). The presence of myocardin is reported from the HH9 (day 1) stage of a developing chick when the cardiomyocyte-fated progenitors start to fuse until the valves and nodes of a developed heart are fully formed (Brand, 2003). MYOCD protein has also been reported to have many structural and functional roles in heart development, such as cell fusion, cardiomyocyte contractibility, and more. (Raphel *et al.*, 2012). In the current study, COX-2 inhibition caused the downregulation of MYOCD compared to control in day two embryos. It has been informed that MYOCD overexpression reduces cell death and promotes tissue repair in a murine model of hindbrain ischemia (Madonna *et al.*, 2013). Therefore, it is believed that reduced MYOCD expression could be an added reason behind the apoptosis and ameliorated morphogenesis in the developing heart tube under the ablated COX-2 activity in day two embryos.

Additionally, transcriptional factor HAND2 is been shown in the early heart field at HH16, and its downregulation leads to abnormal correct ventricle formation (Srivastava *et al.*, 1997). It has also been reported that HAND2 moves to the outflow tract in the later stages of cardiac looping (Tsuchihashi *et al.*, 2011). Here, treatment was observed to decrease HAND2 expression in embryonic heart tissue, which, together with a compromised level of MYOCD, would account for the looping defects noticed in the heart of day two and day three chick embryos.

SHH is another factor that regulates the right and left looping of the heart in early-developing embryos. It turns the heart tube in the right direction, further interacts with HAND, and leads to the maturation of the heart chambers (Tsuda *et al.*, 1998). In our study, SHH gene expression increased on day two under the etoricoxib treatment, while on day three, its levels decreased as compared to respective controls. Deviant expression of the SHH gene leads to disruption in the looping pattern of the cardiac tube, which ultimately causes congenital heart defects in developing embryos. SHH signaling pathways are critical in regulating the normal proliferation and migration rate (Dyer and Kirby, 2009).

In this respect, the member of the TGF- β family BMP4 is also known to control cardiac cell proliferation and differentiation by interacting with Wnt (Ye *et al.*, 2019). Reports showed that BMP4 provides the left-right integrity of heart structure in developing zebrafish embryos (Chen *et al.*, 1997). The expression level of BMP4 was found to decrease in the treated group of day two and day three embryos. Subsided level of BMP4 suggests its reduced interaction with Wnt and their downstream molecules, leading to defective patterning of the heart tube.

The cardiomyocyte population has to be maintained for sculpting the heart tube. During heart tube development, the cardiomyocytes are in constantly proliferate (Linask *et al.*, 2005). Initially, when a heart tube is formed, the apoptosis is found to be minimal; however, when the heart tube starts differentiating into chambers, the apoptosis rate in cardiomyocytes increases (Zhao and Rivkees, 2000). The ratio of proliferation and apoptosis maintains the cell number and progress of heart development. The level of PCNA in the etoricoxib-treated embryo decreased drastically, while that of Cl.Caspase3 increased, leading to fewer cells, as seen in the histology of heart sections.

Overall, due to COX-2 inhibition, a significant signaling molecule like Wnt11 was affected along with its downstream targets, such as GATAs and TBXs, which are interconnected for the heart tube patterning. Alteration in these might have resulted in the malformation of the heart in the chick embryo.

COX-2 inhibition resulted in heart tube looping alterations and defective trabeculation in the ventricular region of day two and day three chick embryos. The regulatory molecules were affected when levels of COX-2 went down. Alterations at gene and protein levels were reflected in the morphology of the developing heart. Our findings with chick embryos suggested that COX-2 has a crucial role in patterning the heart in vertebrates.

Materials and Methods

Animal procurement and maintenance

This study used the fertilized eggs of the Rhode Island Red (RIR) breed of domestic chicken. They were obtained from the Intensive Poultry Development Unit, Vadodara, Gujarat, India. Prior to incuba-

tion, eggs were candled to visualize the air sac and wiped with a povidone-iodine solution. All experiments were carried out per the committee's guidelines for controlling and supervising experiments on animals (CPCSEA). The institutional animal ethics committee approved the protocols (IAEC No. MSU-Z/IAEC/09-2020).

Experiment design

Freshly laid eggs were categorized into two different groups, control, and treatment, randomly after disinfecting with povidone-iodine solution. All the experiments were performed thrice with 30 eggs in each group. Control and treatment groups of eggs were punctured at the marked air sac region with a sterile needle under the laminar airflow (LAF). In the control group of eggs, 50 µl of Mili-Q water was dispensed. For the treatment group, the same volume of 70 mg/ml (Low observed effective concentration-LOEC) etoricoxib prepared in Mili-Q water was administered. Thus, each treated embryo received 3.5 µg of etoricoxib dissolved in water.

All the experimental eggs were kept in an automated incubator at 37.5±0.5°C and relative humidity of 70-75% (Forma environmental chamber, Thermo Scientific USA). The eggs are automatically rotated every hour and incubated until the desired day embryos are isolated.

Embryo collection

Embryos were harvested on predetermined days, where their growth stages were confirmed by following Hamburger Hamilton (HH) stages of chick development (Hamburger and Hamilton, 1951). Embryos belonging to HH stage 12 (day 2) and HH stage 20 (day 3) were used for further experimentation and analysis.

Immunohistochemistry

The control embryos of day 2 (HH12) and day 3 (HH20) were fixed with 4% PFA at room temperature for 1 hour, followed by sucrose gradient then OCT was used for embedding. 10µm thick sections were taken through the heart region of the embryos using a cryostat (Reichert-Jung, cryo-cut). The sectioned embryos were rehydrated and washed with PBS, and then they were permeabilized at room temperature for 30 minutes and blocked. The embryo sections were blocked with Genei blocking solution for one hour (Genei Laboratories Private Limited, India). The sections were incubated at 4 °C overnight with rabbit anti-COX-2 antibody (1:500 dilution) (Sigma-Aldrich, USA, SAB4200576) and rabbit anti-CI.Caspase3 antibody (1:500 dilution) (Sigma-Aldrich, USA, C8487) followed by secondary antibody goat anti-rabbit Alexa 488 (Invitrogen, USA, Cat no. A-11008) (1:1000 dilution) for one hour at room temperature in dark condition. Sections were incubated with nuclear stain DAPI (Invitrogen, USA, Cat no. D1306) for 10 minutes, followed by a wash with PBST and mounted on using Fluoromount. Imaging was done using Zeiss LSM-710 confocal microscope and analyzed in ImageJ software.

COX activity assay

The heart tissues were collected from both groups on day two and day three in 0.1 M Tris-EDTA buffer, and 10% homogenate of tissue was used to estimate COX-2 activity following the manufacturer's protocol (Cayman Chemical, USA).

A selective COX-1 inhibitor SC-560 was used for inhibitory wells. All the wells have assay buffer and heme along with samples (standard, background, and inhibitory wells). The plate was incubated

TABLE 1

PRIMER SEQUENCE

Gene	Forward primer	Reverse primer	Accession number
WNT11	GACCTGGGTATCGATGGGGA	GGCTTTCAGACCTGTCTCC	NM_204784
GATA4	GGCATGCCAACATCGAATTTTT	CTTGCCGGGGTACTGTGAG	NM_001293106
GATA5	GGCAAAACCTCAACAGGGTC	CTTGCCGGGGTACTGTGAG	NM_205421
GATA6	GCGCCCTACGACGGATCTC	GGGTGGTGGGCACGTAGAC	NM_205420
TBX20	GATATGCCTACCACCGCTCC	CGTAGAGCCTTGCTGGGAGA	NM_204144
MYOCD	GTCCCCCAACAGCCACTATC	CGTAGAGCCTTGCTGGGAGA	NM_001080715
HAND2	AGCGGCGATGAGTCTTGTG	CAGCCGTGAAGTAGGGGTTTC	NM_204966
SHH	TGCTAGGATCGGTGGATAG	ACAAGTCAGCCAGAGGAGA	NM_204821
BMP4	TGGAAGAACGTGCCATCGC	AGACTGGCATGTTGGCTCTC	NM_205237
PCNA	TGTTCTCTCGTTGTGGAGT	TCCCAGTCAGTTAAGAGCC	NM_204170
CASP3	AAAGATGGACCACGCTCAGG	TGACAGTCGGTATCTCGGT	NM_204725
18s rRNA	GGCCGTTCTTAGTTGGTGGGA	GGCCGTTCTTAGTTGGTGGGA	XR_005840267

for 10 minutes at room temperature, and 20 µl of the calorimetric substrate was added last. Absorbance was measured at 590 nm, which is the absorbance maxima of oxidized N,N,N',N'-Tetramethyl-p-phenylenediamine (TMPD) corresponding amount of peroxidase activity of COX-2 enzyme. COX-2 activity was calculated with reference to the total protein in a sample. An unpaired t-test was performed to determine the significance values between the control and treatment groups.

q-RT PC

Heart tissues were collected from the isolated embryos of both control and treatment groups. Total RNA was isolated from heart tissue using the TRIzol method and quantified through Qubit assay on a Qubit 3.0 fluorimeter (Life Technologies, USA). One µg of isolated RNA was used to prepare cDNA using a high-capacity reverse transcription kit (Applied Biosystems, Thermo Fisher Scientific, USA). Quantitative RT-PCR was performed using LightCycler96 (Roche Diagnostics, USA) as per the following protocol: 32 cycles consisting of denaturation at 95 °C for 10 sec., annealing at 60 °C for 30 seconds, and extension at 72 °C for 30 seconds. The specific products were confirmed by analyzing their melting curves.

Cq values were used for fold change calculation and represented as $2^{-\Delta\Delta Cq}$ according to Livak and Schmittgen (Livak and Schmittgen, 2001). The internal control was 18s rRNA for this experiment. Primers were designed using the online primer blast tool from NCBI (Table 1).

In order to minimize biological variation, tissue samples collected from three embryos were pooled, and each variable was analyzed by q-RT PCR, three technical replicates were performed to reduce experimental errors.

Protein expression analysis

Western blot was performed to determine relative protein expression in various groups. Heart tissue was collected from control and treated embryos on days two and three. The tissue was homogenized in lysis buffer with protease inhibitor. Total protein was isolated and quantified by Bradford's assay (Bradford, 1976). 30 µg of total protein was electrophoresed on a 12% polyacrylamide gel and transferred to PVDF membrane, which was then immunostained for MYOCD (Anti-MYOCD IgG raised in mouse, Sigma Aldrich, USA, SAB4200539), PCNA (Anti-PCNA IgG raised in rabbit, Sigma Aldrich, USA, SAB2108448) and CI.Caspase3 (Anti-CI.Caspase3 IgG raised in rabbit, Sigma Aldrich, USA, C8487) using

primary antibodies diluted 1:1000 times in assay buffer. GAPDH (Anti-GAPDH IgG raised in mouse, Sigma Aldrich, USA) was used as an internal control. Biotinylated secondary polyclonal antibody IgG (Sigma Aldrich, USA, B8895) type was used and probed using ALP-BCIP-NBT for color development of the blots. The blots' band intensity was measured by densitometry analysis using ImageJ (Supplementary data).

Histological study

Day three control and etoricoxib-treated embryos were isolated using the filter ring method, then rinsed in PBS and fixed in 10% neutral buffer formalin. The tissue was further processed for paraffin wax block preparation. Transverse sections of the heart region were taken using a microtome. These sections were subsequently stained with Harris Hematoxylin and Eosin (Thermo Fisher Scientific, USA). The histological details of the tissue section were visualized using a Leica DM2500 microscope, and pictures were captured using an EC3 camera (utilizing LAS EZ software).

Acknowledgments

The work was supported by Innovation in Science Pursuit for Inspired Research (INSPIRE) grant (No. IF190305 Dt. 01/12/2020). BP is thankful to SHODH and DST-INSPIRE for providing fellowship. We are grateful to Sun Pharmaceutical Industries Ltd., Vadodara, India, for providing technical grade Etoricoxib (batch no.7090/F/727/36A) as a generous gift. BP is thankful to Neelanjana and Shivangi for confocal imaging.

Competing interests

The authors declare that no competing interests exist.

Author contributions

Bhaval Parmar: Investigation, Data curation, Writing – original draft. Urja Verma: Data curation. Juhi Vaishnav: Data curation. Suresh Balakrishnan: Conceptualization, Methodology, Writing – review & editing.

References

- BARTELINKS M. M., GITTEBERGER-DE GROOT A. C. (1989). The outflow tract of the heart – embryologic and morphologic correlations. *International Journal of Cardiology* 22: 289-300. [https://doi.org/10.1016/0167-5273\(89\)90270-2](https://doi.org/10.1016/0167-5273(89)90270-2)
- BONDESEN B. A., MILLS S. T., PAVLATH G. K. (2006). The COX-2 pathway regulates growth of atrophied muscle via multiple mechanisms. *American Journal of Physiology-Cell Physiology* 290: C1651-C1659. <https://doi.org/10.1152/ajpcell.00518.2005>
- BRADFORD M. M. (1976). A rapid and sensitive method for the quantitation of microgram quantities of protein utilizing the principle of protein-dye binding. *Analytical Biochemistry* 72: 248-254. [https://doi.org/10.1016/0003-2697\(76\)90527-3](https://doi.org/10.1016/0003-2697(76)90527-3)
- BRAND T. (2003). Heart development: molecular insights into cardiac specification and early morphogenesis. *Developmental Biology* 258: 1-19. [https://doi.org/10.1016/S0012-1606\(03\)00112-X](https://doi.org/10.1016/S0012-1606(03)00112-X)
- BROWN D. D., MARTZ S. N., BINDER O., GOETZ S. C., PRICE B. M. J., SMITH J. C., CONLON F. L. (2005). Tbx5 and Tbx20 act synergistically to control vertebrate heart morphogenesis. *Development* 132: 553-563. <https://doi.org/10.1242/dev.01596>
- BUCH P. R., SARKATE P., UGGINI G. K., DESAI I., BALAKRISHNAN S. (2017). Inhibition of Cyclooxygenase-2 Alters Wnt/ β -Catenin Signaling in the Regenerating Tail of Lizard *Hemidactylus flaviviridis*. *Tissue Engineering and Regenerative Medicine* 14: 171-178. <https://doi.org/10.1007/s13770-017-0037-2>
- CHEN J.F., WANG S., WU Q., CAO D., NGUYEN T., CHEN Y., WANG D.Z. (2008). Myocardin Marks the Earliest Cardiac Gene Expression and Plays an Important Role in Heart Development. *The Anatomical Record: Advances in Integrative Anatomy and Evolutionary Biology* 291: 1200-1211. <https://doi.org/10.1002/ar.20756>
- CHEN J. (2000). Genetics of heart development. *Trends in Genetics* 16: 383-388. [https://doi.org/10.1016/S0168-9525\(00\)02075-8](https://doi.org/10.1016/S0168-9525(00)02075-8)
- CHEN J.N., VAN EEDEN F.J., WARREN K.S., CHIN A., NUSSLEIN-VOLHARD C., HAFFTER P., FISHMAN M.C. (1997). Left-right pattern of cardiac BMP4 may drive asymmetry of the heart in zebrafish. *Development* 124: 4373-4382. <https://doi.org/10.1242/dev.124.21.4373>
- DEES E., LIN H., COTTON R. B., GRAHAM T. P., DODD D. A. (2000). Outcome of preterm infants with congenital heart disease. *The Journal of Pediatrics* 137: 653-659. <https://doi.org/10.1067/mpd.2000.108568>
- DYER L. A., KIRBY M. L. (2009). Sonic hedgehog maintains proliferation in secondary heart field progenitors and is required for normal arterial pole formation. *Developmental Biology* 330: 305-317. <https://doi.org/10.1016/j.ydbio.2009.03.028>
- EISENBERG C. A., EISENBERG L. M. (1999). WNT11 promotes cardiac tissue formation of early mesoderm. *Developmental Dynamics* 216: 45-58. [https://doi.org/10.1002/\(SICI\)1097-0177\(199909\)216:1<45::AID-DVDY7>3.0.CO;2-L](https://doi.org/10.1002/(SICI)1097-0177(199909)216:1<45::AID-DVDY7>3.0.CO;2-L)
- HAMBURGER V., HAMILTON H. L. (1951). A series of normal stages in the development of the chick embryo. *Journal of Morphology* 88: 49-92. <https://doi.org/10.1002/jmor.1050880104>
- HUANG J., MIN LU M., CHENG L., YUAN L.J., ZHU X., STOUT A. L., CHEN M., LI J., PARMACEK M. S. (2009). Myocardin is required for cardiomyocyte survival and maintenance of heart function. *Proceedings of the National Academy of Sciences* 106: 18734-18739. <https://doi.org/10.1073/pnas.0910749106>
- JANA S., CHATTERJEE K., RAY A. K., DASMAHAPATRA P., SWARNAKAR S. (2016). Regulation of Matrix Metalloproteinase-2 Activity by COX-2-PGE2-pAKT Axis Promotes Angiogenesis in Endometriosis. *PLOS ONE* 11: e0163540. <https://doi.org/10.1371/journal.pone.0163540>
- KHOSHNOOD B., LELONG N., HOUYEL L., THIEULIN A.C., JOUANNIC J.M., MAGNIER S., DELEZOIDE A.L., MAGNY J.F., RAMBAUD C., BONNET D., GOFFINET F. (2012). Prevalence, timing of diagnosis and mortality of newborns with congenital heart defects: a population-based study. *Heart* 98: 1667-1673. <https://doi.org/10.1136/heartjnl-2012-302543>
- LAFORST B., ANDEFINGER G., NEMER M. (2011). Loss of Gata5 in mice leads to bicuspid aortic valve. *Journal of Clinical Investigation* 121: 2876-2887. <https://doi.org/10.1172/JCI44555>
- LAFORST B., NEMER M. (2011). GATA5 interacts with GATA4 and GATA6 in outflow tract development. *Developmental Biology* 358: 368-378. <https://doi.org/10.1016/j.ydbio.2011.07.037>
- LAURENT F., GIRDIUSAITE A., GAMART J., BAROZZI I., OSTERWALDER M., AKIYAMA J. A., LINCOLN J., LOPEZ-RIOS J., VISEL A., ZUNIGA A., ZELLER R. (2017). HAND2 Target Gene Regulatory Networks Control Atrioventricular Canal and Cardiac Valve Development. *Cell Reports* 19: 1602-1613. <https://doi.org/10.1016/j.celrep.2017.05.004>
- LEPORE J. J. (2006). GATA-6 regulates semaphorin 3C and is required in cardiac neural crest for cardiovascular morphogenesis. *Journal of Clinical Investigation* 116: 929-939. <https://doi.org/10.1172/JCI27363>
- LINASK K. K., HAN M., CAI D. H., BRAUER P. R., MAISAstry S. M. (2005). Cardiac morphogenesis: Matrix metalloproteinase coordination of cellular mechanisms underlying heart tube formation and directionality of looping. *Developmental Dynamics* 233: 739-753. <https://doi.org/10.1002/dvdy.20377>
- LIVAK K. J., SCHMITTGEN T. D. (2001). Analysis of Relative Gene Expression Data Using Real-Time Quantitative PCR and the 2 $\Delta\Delta$ CT Method. *Methods* 25: 402-408. <https://doi.org/10.1006/meth.2001.1262>
- LOPEZ-SANCHEZ C., GARCIA-MASA N., GANAN C. M., GARCIA-MARTINEZ V. (2009). Movement and commitment of primitive streak precardiac cells during cardiogenesis. *The International Journal of Developmental Biology* 53: 1445-1455. <https://doi.org/10.1387/ijdb.072417cl>
- LUTIN W.A., BRUMUND M.R., JONES C., THARPE C.E., MONTEGOMERY M., MCCAFFREY F.M. (1999). Hemodynamic Abnormalities in Fetuses with Congenital Heart Disease. *Pediatric Cardiology* 20: 390-395. <https://doi.org/10.1007/s002469900497>
- MADONNA R., TAYLOR D. A., GENG Y.J., DE CATERINA R., SHELAT H., PERIN E. C., WILLERSON J. T. (2013). Transplantation of Mesenchymal Cells Rejuvenated by the Overexpression of Telomerase and Myocardin Promotes Revascularization and Tissue Repair in a Murine Model of Hindlimb Ischemia. *Circulation Research* 113: 902-914. <https://doi.org/10.1161/CIRCRESAHA.113.301690>
- MOLKENTIN J. D., LIN Q., DUNCAN S. A., OLSON E. N. (1997). Requirement of the transcription factor GATA4 for heart tube formation and ventral morphogenesis. *Genes & Development* 11: 1061-1072. <https://doi.org/10.1101/gad.11.8.1061>

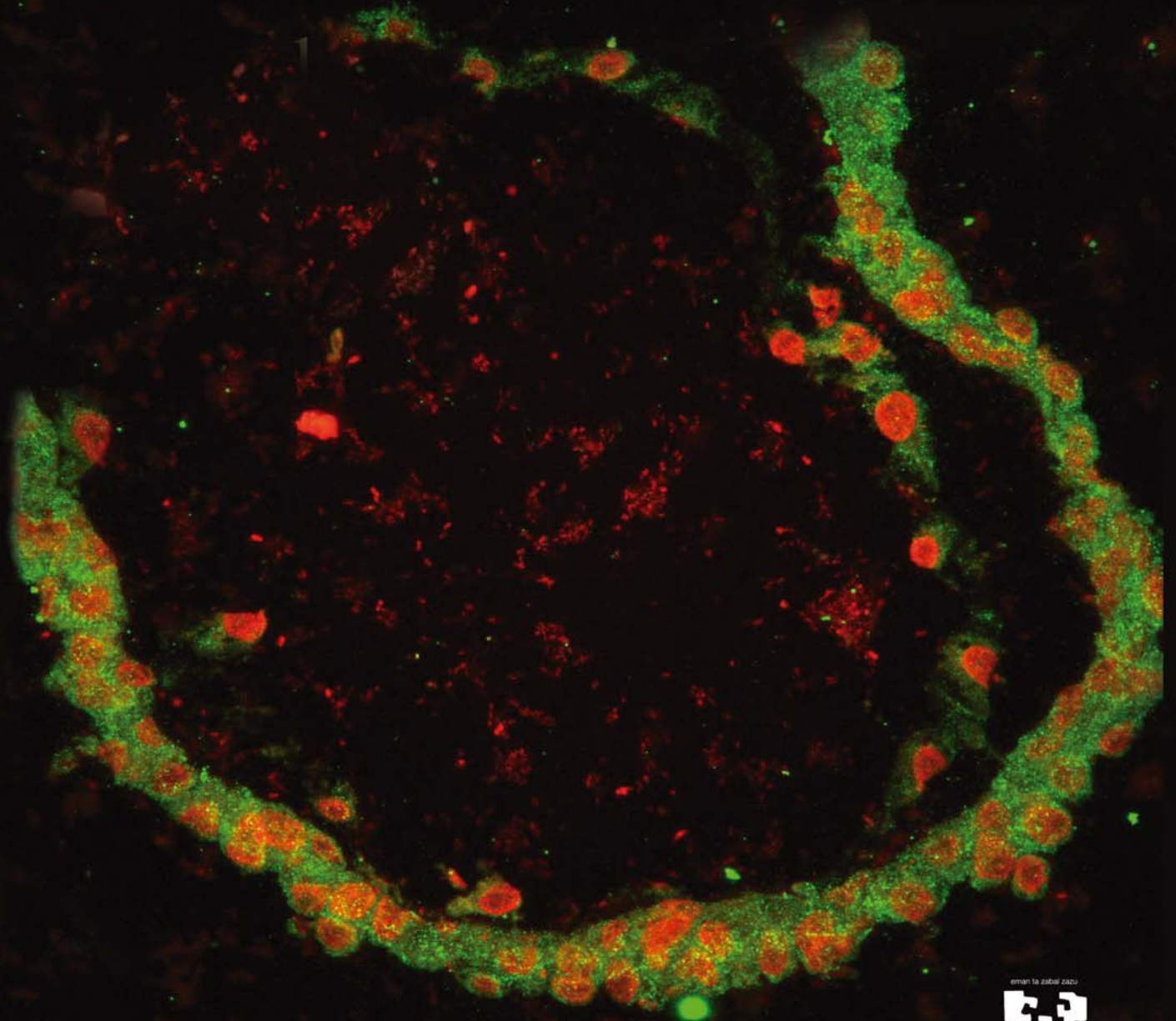
- NARITA N., BIELINSKA M., WILSON D.B. (1997). Cardiomyocyte differentiation by GATA-4-deficient embryonic stem cells. *Development* 124: 3755-3764. <https://doi.org/10.1242/dev.124.19.3755>
- NEIL J. R., JOHNSON K. M., NEMENOFF R. A., SCHIEMANN W. P. (2008). Cox-2 inactivates Smad signaling and enhances EMT stimulated by TGF- through a PGE2-dependent mechanisms. *Carcinogenesis* 29: 2227-2235. <https://doi.org/10.1093/carcin/bgn202>
- NEMER M. (2008). Genetic insights into normal and abnormal heart development. *CardiovascularPathology* 17: 48-54. <https://doi.org/10.1016/j.carpath.2007.06.005>
- NØRREGAARD R., KWON T.H., FRØKIÆR J. (2015). Physiology and pathophysiology of cyclooxygenase-2 and prostaglandin E2 in the kidney. *Kidney Research and Clinical Practice* 34: 194-200. <https://doi.org/10.1016/j.krcp.2015.10.004>
- OLSON E. N. (2006). Gene Regulatory Networks in the Evolution and Development of the Heart. *Science* 313: 1922-1927. <https://doi.org/10.1126/science.1132292>
- PAKRASI P. L., JAIN A. K. (2008). Cyclooxygenase-2-derived endogenous prostacyclin reduces apoptosis and enhances embryo viability in mouse. *Prostaglandins, Leukotrienes and Essential Fatty Acids* 79: 27-33. <https://doi.org/10.1016/j.plefa.2008.07.006>
- PANDUR P., LÄSCHE M., EISENBERG L. M., KÜHL M. (2002). Wnt-11 activation of a non-canonical Wnt signalling pathway is required for cardiogenesis. *Nature* 418: 636-641. <https://doi.org/10.1038/nature00921>
- PÉREZ-POMARES J. M., DE LA POMPA J. L. (2011). Signaling During Epicardium and Coronary Vessel Development. *Circulation Research* 109: 1429-1442. <https://doi.org/10.1161/CIRCRESAHA.111.245589>
- PETERKIN T., GIBSON A., PATIENT R. (2007). Redundancy and evolution of GATA factor requirements in development of the myocardium. *Developmental Biology* 311: 623-635. <https://doi.org/10.1016/j.ydbio.2007.08.018>
- PIVEN O. O., WINATA C. L. (2017). The canonical way to make a heart: β -catenin and plakoglobin in heart development and remodeling. *Experimental Biology and Medicine* 242: 1735-1745. <https://doi.org/10.1177/1535370217732737>
- PLAGEMAN T. F., YUTZEY K. E. (2004). Differential Expression and Function of Tbx5 and Tbx20 in Cardiac Development. *Journal of Biological Chemistry* 279: 19026-19034. <https://doi.org/10.1074/jbc.M314041200>
- RANDALL C. L., ANTON R. F., BECKER H. C., HALE R. L., EKBLAD U. (1991). Aspirin dose-dependently reduces alcohol-induced birth defects and prostaglandin E levels in mice. *Teratology* 44: 521-529. <https://doi.org/10.1002/tera.1420440506>
- RAPHEL L., TALASILA A., CHEUNG C., SINHA S. (2012). Myocardin Overexpression Is Sufficient for Promoting the Development of a Mature Smooth Muscle Cell-Like Phenotype from Human Embryonic Stem Cells. *PLoS ONE* 7: e44052. <https://doi.org/10.1371/journal.pone.0044052>
- RICCIOTTI E., FITZGERALD G. A. (2011). Prostaglandins and Inflammation. *Arteriosclerosis, Thrombosis, and Vascular Biology* 31: 986-1000. <https://doi.org/10.1161/ATVBAHA.110.207449>
- SHIM M., FOLEY J., ANNA C., MISHINA Y., ELING T. (2010). Embryonic Expression of Cyclooxygenase-2 Causes Malformations in Axial Skeleton. *Journal of Biological Chemistry* 285: 16206-16217. <https://doi.org/10.1074/jbc.M109.078576>
- SINGH M. K., LI Y., LI S., COBB R. M., ZHOU D., LU M. M., EPSTEIN J. A., MORRISEY E. E., GRUBER P. J. (2010). Gata4 and Gata5 Cooperatively Regulate Cardiac Myocyte Proliferation in Mice. *Journal of Biological Chemistry* 285: 1765-1772. <https://doi.org/10.1074/jbc.M109.038539>
- SRIVASTAVA D., THOMAS T., LIN Q., KIRBY M. L., BROWN D., OLSON E. N. (1997). Regulation of cardiac mesodermal and neural crest development by the bHLH transcription factor, dHAND. *Nature Genetics* 16: 154-160. <https://doi.org/10.1038/ng0697-154>
- STENNARD F. A., COSTA M. W., ELLIOTT D. A., RANKIN S., HAAST S. J.P., LAI D., MCDONALD L. P.A., NIEDERREITHER K., DOLLE P., BRUNEAU B. G., ZORN A. M., HARVEY R. P. (2003). Cardiac T-box factor Tbx20 directly interacts with Nkx2-5, GATA4, and GATA5 in regulation of gene expression in the developing heart. *Developmental Biology* 262: 206-224. [https://doi.org/10.1016/S0012-1606\(03\)00385-3](https://doi.org/10.1016/S0012-1606(03)00385-3)
- TSUCHIHASHI T., MAEDA J., SHIN C. H., IVEY K. N., BLACK B. L., OLSON E. N., YAMAGISHI H., SRIVASTAVA D. (2011). Hand2 function in second heart field progenitors is essential for cardiogenesis. *Developmental Biology* 351: 62-69. <https://doi.org/10.1016/j.ydbio.2010.12.023>
- TSUDA T., MAJUMDER K., LINASK K. K. (1998). Differential expression of flectin in the extracellular matrix and left-right asymmetry in mouse embryonic heart during looping stages. *Developmental Genetics* 23: 203-214. [https://doi.org/10.1002/\(SICI\)1520-6408\(1998\)23:3<203::AID-DVG6>3.0.CO;2-6](https://doi.org/10.1002/(SICI)1520-6408(1998)23:3<203::AID-DVG6>3.0.CO;2-6)
- VAN BERLO J. H., MAILLET M., MOLKENTIN J. D. (2013). Signaling effectors underlying pathologic growth and remodeling of the heart. *Journal of Clinical Investigation* 123: 37-45. <https://doi.org/10.1172/JCI62839>
- VAN DEN HOFF M. J.B., MOORMAN A. F.M., RUIJTER J. M., LAMERS W. H., BENNINGTON R. W., MARKWALD R. R., WESSELS A. (1999). Myocardialization of the Cardiac Outflow Tract. *Developmental Biology* 212: 477-490. <https://doi.org/10.1006/dbio.1999.9366>
- VERMA U., GAUTAM M., PARMAR B., KHAIRE K., WISHART D. S., BALAKRISHNAN S. (2021). New insights into the obligatory nature of cyclooxygenase-2 and PGE2 during early chick embryogenesis. *Biochimica et Biophysica Acta (BBA) - Molecular and Cell Biology of Lipids* 1866: 158889. <https://doi.org/10.1016/j.bbalip.2021.158889>
- XU D., BU J., GU S., XIA Y., DU J., WANG Y. (2011). Celecoxib Impairs Heart Development via Inhibiting Cyclooxygenase-2 Activity in Zebrafish Embryos. *Anesthesiology* 114: 391-400. <https://doi.org/10.1097/ALN.0b013e3182039f22>
- YE B., LI L., XU H., CHEN Y., LI F. (2019). Opposing roles of TCF7/LEF1 and TCF7L2 in cyclin D2 and Bmp4 expression and cardiomyocyte cell cycle control during late heart development. *Laboratory Investigation* 99: 807-818. <https://doi.org/10.1038/s41374-019-0204-2>
- YELBUZ T. M., WALDO K. L., KUMISKI D. H., STADTH. A., WOLFER R., LEATHERBURY L., KIRBY M. L. (2002). Shortened Outflow Tract Leads to Altered Cardiac Looping After Neural Crest Ablation. *Circulation* 106: 504-510. <https://doi.org/10.1161/01.CIR.0000023044.44974.8A>
- ZHAO Z., RIVKEES S. A. (2000). Programmed cell death in the developing heart: Regulation by BMP4 and FGF2. *Developmental Dynamics* 217: 388-400. [https://doi.org/10.1002/\(SICI\)1097-0177\(200004\)217:4<388::AID-DVDY6>3.0.CO;2-N](https://doi.org/10.1002/(SICI)1097-0177(200004)217:4<388::AID-DVDY6>3.0.CO;2-N)

Image from the article Parmar et al., 2022 published as the IJDB coverpage

THE INTERNATIONAL JOURNAL OF DEVELOPMENTAL BIOLOGY

Volume 66 Nos. 7/8/9

2022



Cyclooxygenase-2 and the chamber of secrets: The developing heart of a chick, stained for the presence of previously unknown cyclooxygenase-2. (COX-2 in green and nucleus in red).

Appendix 1 Publications from thesis

emman la zabal zazu



Universidad
del País Vasco

Euskal Herriko
Unibertsitatea

Article

Inhibition of Cyclooxygenase-2 Alters Craniofacial Patterning during Early Embryonic Development of Chick

Bhaval Parmar, Urja Verma, Kashmiri Khair, Dhanush Danes, Suresh Balakrishnan *

Department of Zoology, Faculty of Science, The Maharaja Sayajirao University of Baroda, Gujarat 390002, India; bhaval.p-zoophd@msubaroda.ac.in (B.P.); urja.verma-zoophd@msubaroda.ac.in (U.V.); kashmira.k-zoophd@msubaroda.ac.in (K.K.); dhanush.danes-zoo@msubaroda.ac.in (D.D.)

* Correspondence: b.suresh-zoo@msubaroda.ac.in

Abstract: A recent study from our lab revealed that the inhibition of cyclooxygenase-2 (COX-2) exclusively reduces the level of PGE₂ (Prostaglandin E₂) among prostanoids and hampers the normal development of several structures, strikingly the cranial vault, in chick embryos. In order to unearth the mechanism behind the deviant development of cranial features, the expression pattern of various factors that are known to influence cranial neural crest cell (CNCC) migration was checked in chick embryos after inhibiting COX-2 activity using etoricoxib. The compromised level of cell adhesion molecules and their upstream regulators, namely CDH1 (E-cadherin), CDH2 (N-cadherin), MSX1 (Msh homeobox 1), and TGF- β (Transforming growth factor beta), observed in the etoricoxib-treated embryos indicate that COX-2, through its downstream effector PGE₂, regulates the expression of these factors perhaps to aid the migration of CNCCs. The histological features and levels of FoxD3 (Forkhead box D3), as well as PCNA (Proliferating cell nuclear antigen), further consolidate the role of COX-2 in the migration and survival of CNCCs in developing embryos. The results of the current study indicate that COX-2 plays a pivotal role in orchestrating craniofacial structures perhaps by modulating CNCC proliferation and migration during the embryonic development of chicks.

Keywords: cranial neural crest cells; embryogenesis; development; cell migration

Citation: Parmar, B.; Verma, U.; Khair, K.; Danes, D.; Balakrishnan, S. Inhibition of Cyclooxygenase-2 Alters Cranial Neural Crest Cell Migration in the developing chick. *J. Dev. Biol.* **2021**, *9*, 16. <https://doi.org/10.3390/jdb9020016>

Academic Editors: Simon J. Conway and Sally Moody

Received: 27 February 2021

Accepted: 20 April 2021

Published: 23 April 2021

Publisher's Note: MDPI stays neutral with regard to jurisdictional claims in published maps and institutional affiliations.



Copyright: © 2021 by the authors. Licensee MDPI, Basel, Switzerland. This article is an open access article distributed under the terms and conditions of the Creative Commons Attribution (CC BY) license (<http://creativecommons.org/licenses/by/4.0/>).

1. Introduction

Craniofacial development involves the formation of cranial neural crest cells (CNCCs) via epithelial–mesenchymal transition (EMT), induction, delamination, and migration, followed by the morphogenesis of various organs of an organism [1]. The above-mentioned events are tightly regulated by several genes that coordinate for craniofacial formation and patterning [2]. CNCCs are clusters of multipotent cells and fate-restricted progenitors that can differentiate into a multitude of tissue types based on the molecular signals they receive [3]. Their precursors undergo EMT and migrate from the forebrain, midbrain, and rhombomeres of the hindbrain to populate at the pharyngeal arches and contribute to the patterning of head and face structures. Once CNCCs pass through the EMT process, they begin migration. During migration, they proliferate and increase the pool of cells. The whole process of CNCC migration and proliferation is governed by various signaling pathways such as Fgf (Fibroblast growth factors), Wnt (Wingless-related integration site), TGF- β , and BMP (Bone morphogenetic protein) [3,4]. When the migration or differentiation of CNCCs is disrupted, defects of descendant tissues occur, which result in craniofacial malformations, the most common birth defect in humans [5].

Based on studies involving a wide array of model organisms, it can be construed that the molecular organizers of CNCC migration are conserved across various classes of vertebrates [4,6,7]. The canonical Wnt/ β -catenin signaling pathway is reported to play a major role in the formation and progression of CNCCs, as it influences both delamination

and migration by interacting with BMP4 and TGF- β , respectively [8–11]. Delamination is a collective effort orchestrated by downstream targets of Wnt3A and BMP4 signaling. Interestingly, BMP also plays a pivotal role in the specification of CNCCs into glial cell lineages [12]. However, the proximate regulators of TGF- β such as Snail1 (Zinc finger protein SNAI1), Twist, MSX1, MSX2, and Sox9 (SRY-related HMG-box genes) maintain the pluripotency of CNCCs during migration. Additionally, TGF- β decreases the levels of E-cadherin, with a concomitant surge in N-cadherin, by regulating the expression of Twist, Snail, and Slug, which triggers the transition of cells from epithelial to mesenchymal lineage in the neural tube [13].

Among the variety of regulatory factors reported to be expressed during delamination and migration, one key molecule is COX-2, an inducible isoform of cyclooxygenase, which catalyzes the formation of PGE₂ from arachidonic acid [14]. COX-2-mediated PGE₂ synthesis plays a crucial role in cellular events such as cell proliferation, migration, EMT, and differentiation by modulating a myriad of signal transduction pathways such as Wnt/ β -catenin, BMP, and TGF- β [15–17]. A study by Jang and coworkers (2009) showed that COX-2 predominantly induces EMT in colon cancer cells by altering the expression of E-cadherin [18]. COX-2 is known to regulate the metastasis of cancerous cells by interacting with TGF- β and its downstream targets [19].

A study from our lab showed that the inhibition of COX-2 by etoricoxib, an NSAID (Nonsteroidal anti-inflammatory drug) specific for the isoform, results in developmental defects in limbs, vascularization, tissue integrity, and the organ patterning of developing chick, where the second most frequently occurring congenital malformations were in the craniofacial region after limb defects [20]. In this study, it was also observed that the selective inhibition of COX-2 reduced only the level of PGE₂, while the remaining prostanooids maintained their normal titer. Based on these findings and the reported possible interactions of COX-2 with different signaling molecules, we hypothesize that the pathways regulating CNCC delamination and migration might be altered due to COX-2 inhibition, resulting in craniofacial defects in developing embryos. In order to validate this notion, in the present study, the activity of COX-2 was inhibited using etoricoxib, a selective COX-2 inhibitor, and its effect on the regulators of CNCC migration and neural tube closure was ascertained in the chicken embryos.

2. Methodology

2.1. Animal Maintenance

Embryos used for experiments were isolated from eggs of the Rhode Island Red (RIR) breed of *Gallus gallus*. RIR eggs were obtained from the Intensive Poultry Development Block (Vadodara, Gujarat, India). Studies were performed in accordance with the guidelines set by the national regulatory authority for experiments on animals, the CPCSEA, and the protocols were approved by the Institutional Animal Ethics Committee (IAEC; No. MSU-Z/IAEC/09-2020).

2.2. Experimental Design

The eggs were randomly divided into control and treatment groups. Before treatment, air cells were marked by candling the eggs, and thereafter, eggs were wiped with povidone–iodine solution. The precise volume of drug or vehicle was administered into the air cells of the eggs by using an insulin syringe in a sterile laminar flow cabinet.

Technical-grade etoricoxib (a generous gift from Sun Pharma Advanced Research Company (Vadodara, India)) was used for the dosing of embryos. The solution of etoricoxib was prepared in Milli-Q water by sonication for 2 h at room temperature. Treatment-group eggs were administered with 50 μ L of 0.07 mg/mL of etoricoxib. A dose of 0.07 mg/mL (lowest observed adverse effect level) was selected based on a previous dose range study conducted in our lab [20]. The final dose concentration injected in each egg was 3.5 μ g (w/v) of etoricoxib. Control-group eggs were treated with 50 μ L of Milli-Q water.

After dosing, eggs were incubated at 37 ± 0.5 °C and $67 \pm 2\%$ relative humidity in a sterile Forma environmental chamber (Thermo Fisher Scientific, USA) until Days 1–3 of embryonic development. These embryos were analyzed for mortality and morphological deformities. For all sets of experiments, 30 and 50 eggs, respectively, were used for control and experimental groups to circumvent treatment-induced variance. The Sun–Shepard formula was used to nullify the differences due to the varied sample sizes among groups [21].

2.3. Histological Study

Embryo isolation was carried out by the filter ring method. The isolated embryos were rinsed with PBS (Phosphate buffered saline) and fixed with 10% neutral buffered formalin. They were further processed, and paraffin wax blocks of the tissue samples were prepared. Transverse sections of Day-2 embryos were taken using a microtome. These sections were subsequently stained with Harris' hematoxylin and eosin (Thermo Fisher Scientific, Waltham, MA, USA). Histological details of the prepared samples were visualized using a Leica DM2500 microscope, and images were captured using an EC3 camera (utilizing LAS EZ software).

2.4. Western Blot

Total protein was isolated from the head region of the embryos using a lysis buffer containing a protease inhibitor under cold conditions. The Bradford method was used for protein quantification. Proteins were resolved by Polyacrylamide gel electrophoresis (PAGE), consisting of 12% resolving and 4% stacking gels. The resolved proteins were transferred on a Polyvinylidene fluoride (PVDF) membrane by the semidry transfer method. The PVDF membrane was immune-stained for N-cadherin, E-cadherin, vimentin, FoxD3, PCNA, cleaved Caspase-3, and Sox2 by using respective monoclonal antibodies (Sigma Aldrich, St. Louis, MO, USA) diluted in assay buffer in 1:1000 ratios. GAPDH (Glyceraldehyde-6-phosphate dehydrogenase) was used as the internal control for protein levels. Biotinylated secondary antibodies were used to generate colored bands on the membrane.

2.5. COX-2 Activity Assay

COX-2 activity was measured by using a kit-based assay (Cayman Chemical, Ann Arbor, MI, USA). The control, treatment, negative control, and positive control were assessed as per the manufacturer's description. Specific activity was calculated by dividing the total protein values derived from the Bradford assay. Statistical significance of the data was calculated by performing a multiple *t*-test.

2.6. RNA Isolation and Quantitative RT-PCR

Total RNA was isolated on Days 1–3 from the head region of embryos using the TRIzol method (Invitrogen, Waltham, MA, USA) and by following the manufacturer's instructions. The One-Step cDNA Synthesis Kit (Applied Biosystems, Foster City, CA, USA) was used to create cDNA from isolated RNA. Gene amplification reactions were performed using Light-Cycler96 (Roche Diagnostics, Rotkreuz, Switzerland) and primers for genes WNT3A, TGFB, CDH1, CDH2, VIM, TWIST, MSX1, PCNA, CASP3, and 18S rRNA (Table 1) to identify their relative quantities in the control and treated embryos. The program was set as follows: 3 min at 95 °C for initial melting, 35 cycles (each cycle of 10 s at 95 °C, 10 s at 60 °C, and 10 s at 72 °C), and a final step of 60 s at 65 °C for extra extension. Melting curves for each well were used to confirm the specificity of the products. 18S rRNA was used as an internal loading control. Mean Cq values of the control gene expression were normalized with the internal control gene expression of each group. Fold change in the expression of both genes compared to the control group was calculated using $2^{-\Delta\Delta Cq}$ values as described by Livak and Schmittgen [22]. Data were analyzed by a Student's *t*-test for significance of the mean difference (GraphPad Software Inc., La Jolla, CA, USA).

Table 1. Oligonucleotide primers used for RT-PCR analysis.

Gene Name	Forward Primer (5'-3')	Reverse Primer (5'-3')	NCBI Ref ID	Product Length (bp)
WNT3A	TCGGAAACTCCCTTTTCAGC	TGCTCATCTTGCCTGGAG	NM_204675.2	106
TGFB	TCGACTTCCGCAAGGATC	CCCGGGTTGTGTTGGTT	HE646744.1	148
CDH1	GAAGACAGCCAAGGGCCTG	TCTGGTACCCTACCCTCTTG	NM_001039258.2	183
CDH2	AGCCAGGAGTTTGTAGTG	TTTGGTCCTTTCTGAGGCC	XM_025147080.1	114
VIM	GACCAGCTGACCAACGA	GAGGCATTGTCAACATCC	NM_001048076.2	158
TWIST	CGAAGCGTTCACGTCGTTAC	TAGCTGCAATTGGTCCCTCG	NM_204739.2	156
MSX1	CTTACATAGGGCCGAGCCG	CAGGCACAGAACAGATCCCA	NM_205488.2	66
PCNA	TGTTCTCTCGTTGTGGAGT	TCCCAGTGCAGTTAAGAGCC	NM_204170.2	105
CASP3	AGTCTTTGGCAGGAAAGCCA	CAAGAGTAATAACCAGGAGCG	XM_015276122.2	195
18S rRNA	GGCCGTTCTTAGTTGGTGGA	TCAATCTCGGGTGGCTGAAC	NR_003278.3	144

3. Results

3.1. COX-2 Activity

Etoricoxib at a dose of 0.07 mg/mL was administered into the air sacks of fertile eggs on Day-0 and to check its inhibitory effects, and a COX-2 activity assay was performed. A significant decrease in COX-2 activity was recorded in the treated embryos during the early developmental stages, namely Hamburger–Hamilton stage 6 (Day-1), HH 12 (Day-2), and HH 20 (Day-3), known for EMT and CNCC migration, respectively, compared to the control group (Figure 1). Further, it was noticed that COX-2 inhibition led to a marginal yet significant increase in the mortality of embryos at all the stages studied, i.e., Days 1–3 (Table 2). Hence, 50 eggs were incubated for each group to ensure the extraction of 30 live embryos for a given experiment.

Table 2. Mortality analysis of chick embryos.

Group	Day-1	Day-2	Day-3
Control	2 (1,4) ***	2 (1,6) ***	3 (2,7) ***
Treatment	10 (8,13)	13 (8,15)	13 (9,15)

Mortality observed on Days 1–3 of embryonic development in the control and etoricoxib-treated groups. Values are expressed as mode with the range in parentheses; *** $p \leq 0.001$.

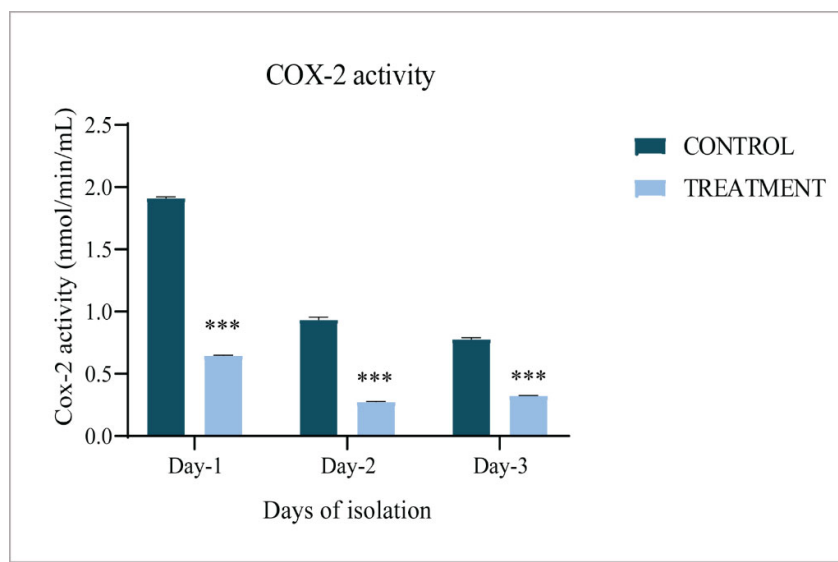


Figure 1. Activity of COX-2 during early development of chick embryos. COX-2 activity in the control and etoricoxib-treated groups of chicks on Days 1–3; *** $p \leq 0.001$.

3.2. Gross Morphology

The sculpting of cranial features coincides with early embryogenesis; hence, the morphology of the cephalic region was studied on Day-1, Day-2, and Day-3 chick embryos. The control-group embryos on Day-1 showed a well-formed neural tube and rhombomeres (Figure 2A), whereas in the treated group, the head fold was disrupted, and the neural tube remained distorted and incompletely formed (Figure 2B–E). Furthermore, on Day-2, embryos of the control group showed defined morphology, with a compact neural tube, perfectly formed rhombomeres, an optic vesicle, and an optic stalk (Figure 3A), while the treated embryos displayed improper closure of the neural tube, a reduced number of somites, and distorted rhombomeres and optic stalks (Figure 3B–D). By the third day, control-group embryos showed a well-structured curved head, perfectly formed optic vesicles, and pharyngeal arches, where neural crest cells further differentiated to form various structures such as frontonasal processes and a mandible (Figure 4A). However, etoricoxib-treated embryos showed a malformed head with no optic vesicle and pharyngeal arches (Figure 4B–D).

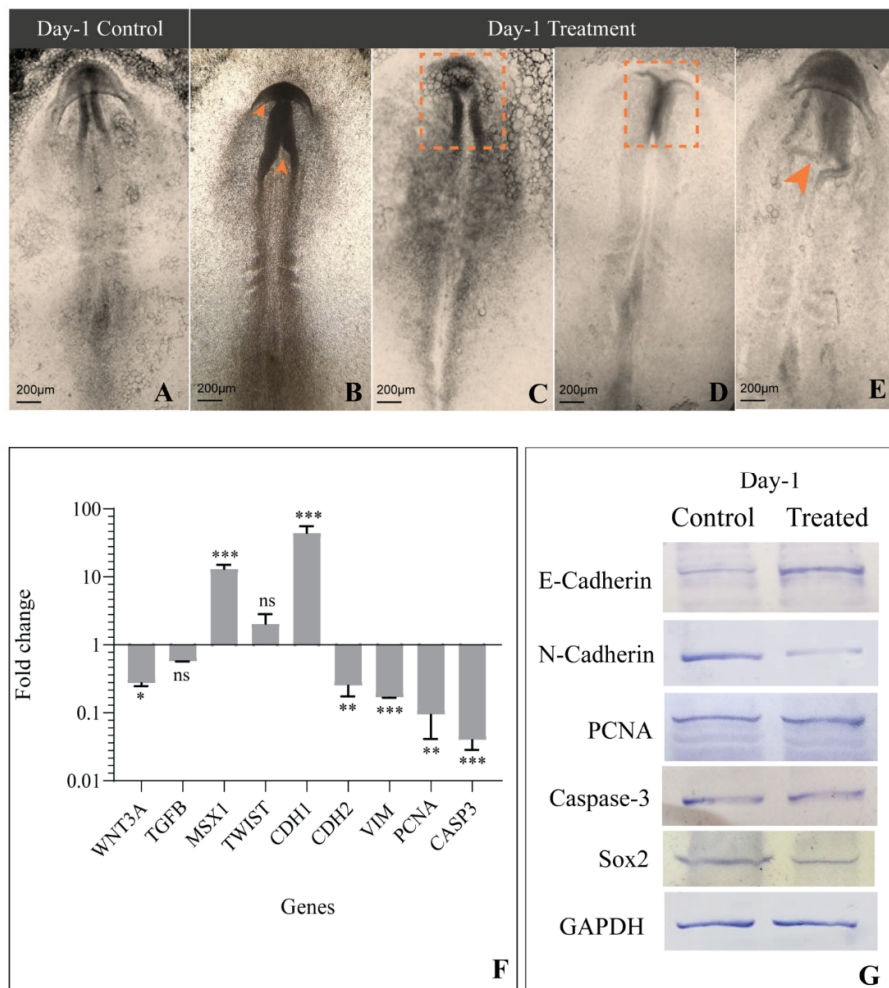


Figure 2. Morphological and molecular aberration due to COX-2 inhibition in the Day-1 embryo. (A) Control embryo with a well-developed neural tube, somite, and neural fold meet at the midbrain level; (B) Etoricoxib-treated embryos have a defective neural fold formation and meet at the forebrain level (orange arrowheads); (C) Etoricoxib-treated embryo showing delayed development and an abnormal neural fold formation (orange dotted square); (D) Fusion of neural folds impaired in the etoricoxib-treated embryo (orange dotted square); (E) Distorted neural fold marked by an orange arrowhead

in the etoricoxib-treated embryo; (F) mRNA expression pattern of the genes involved in regulation of neural crest cell migration in etoricoxib-treated embryo. Values are expressed as fold change (mean ± SEM). Fold change values are compared with the control embryo for all genes (ns: non-significant, *: $p \leq 0.05$, **: $p \leq 0.01$, ***: $p \leq 0.001$); (G) Western blot image showing the comparative expression of various proteins (E-cadherin, N-cadherin, PCNA, Caspase-3 and Sox2) on Day-1. GAPDH was taken as the loading control (n = 3 with 30 eggs per group).

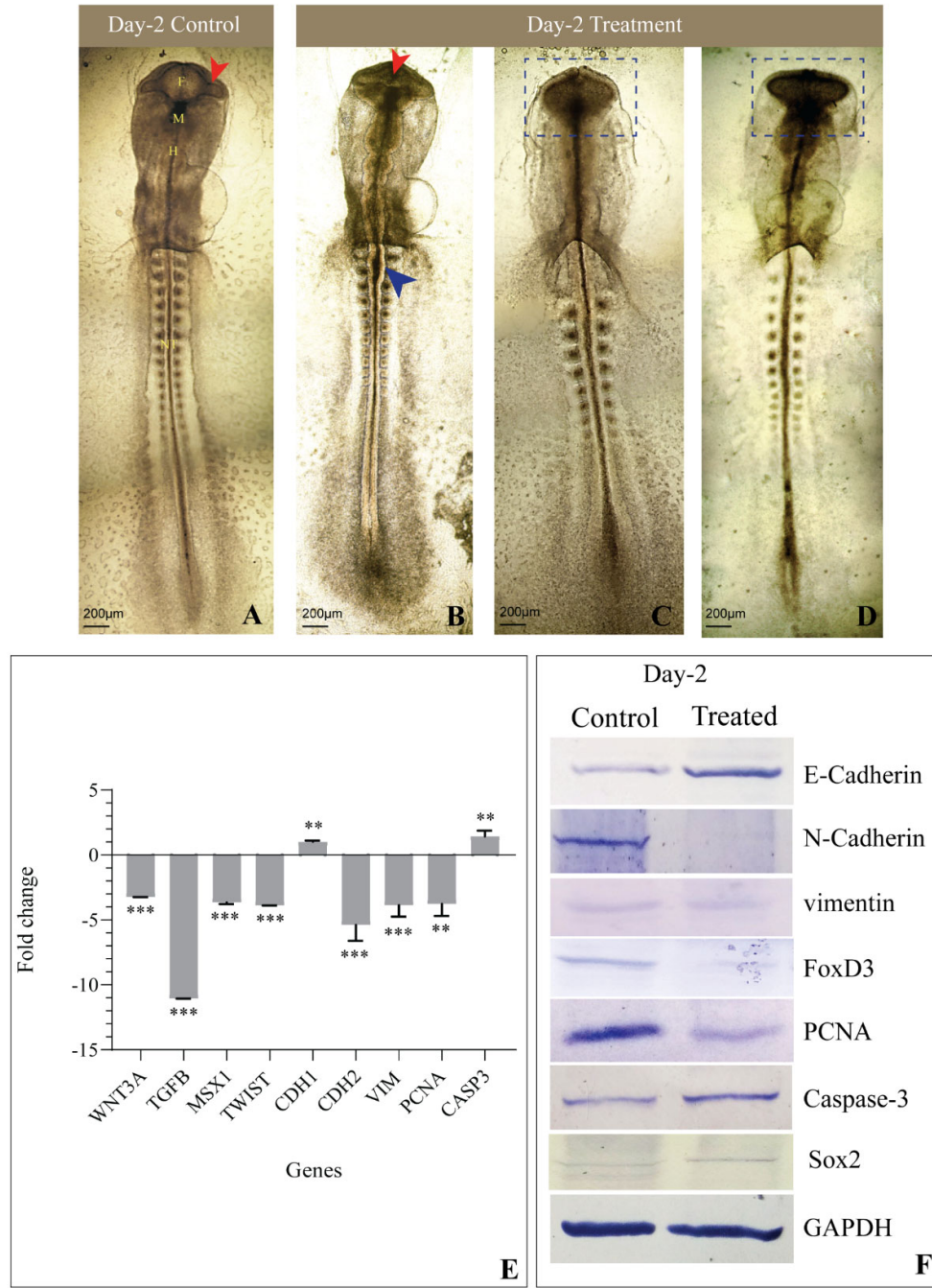


Figure 3. Morphological and molecular changes under COX-2 inhibition in the Day-2 embryo. (A) Control embryo with a well-developed primary optical vesicle and optic stalk (red arrowhead) and three primary brain vesicles are clearly visible (where F—forebrain, H—hindbrain, M—midbrain, and NT—neural tube); (B) Etoricoxib-treated embryo showing an open neural tube (blue arrowhead), incomplete forebrain and optic vesicle (red arrowhead), and a reduced number of somites; (C) The forebrain, midbrain and hindbrain are not formed, with the absence of an optic stalk and an optic vesicle (blue dotted square) in the Day-2 etoricoxib-treated embryo; (D) Deformed forebrain region, optic stalk, and optic vesicle are

not formed (blue dotted square), and fewer somites are formed in the etoricoxib-treated embryo; (E) Transcript-level expression of genes involved in the migration of neural crest cells in etoricoxib-treated Day-2 embryo. Values are expressed as fold change (mean ± SEM). Fold change values of treated embryo are compared with respective controls for all the genes (**: $p \leq 0.01$, ***: $p \leq 0.001$); (F) Western blot image showing the comparative expression of E-cadherin, N-cadherin, FoxD3, vimentin, PCNA, Caspase-3. and Sox2 on Day-2. GAPDH was taken as the loading control (n = 3 with 30 eggs per group).

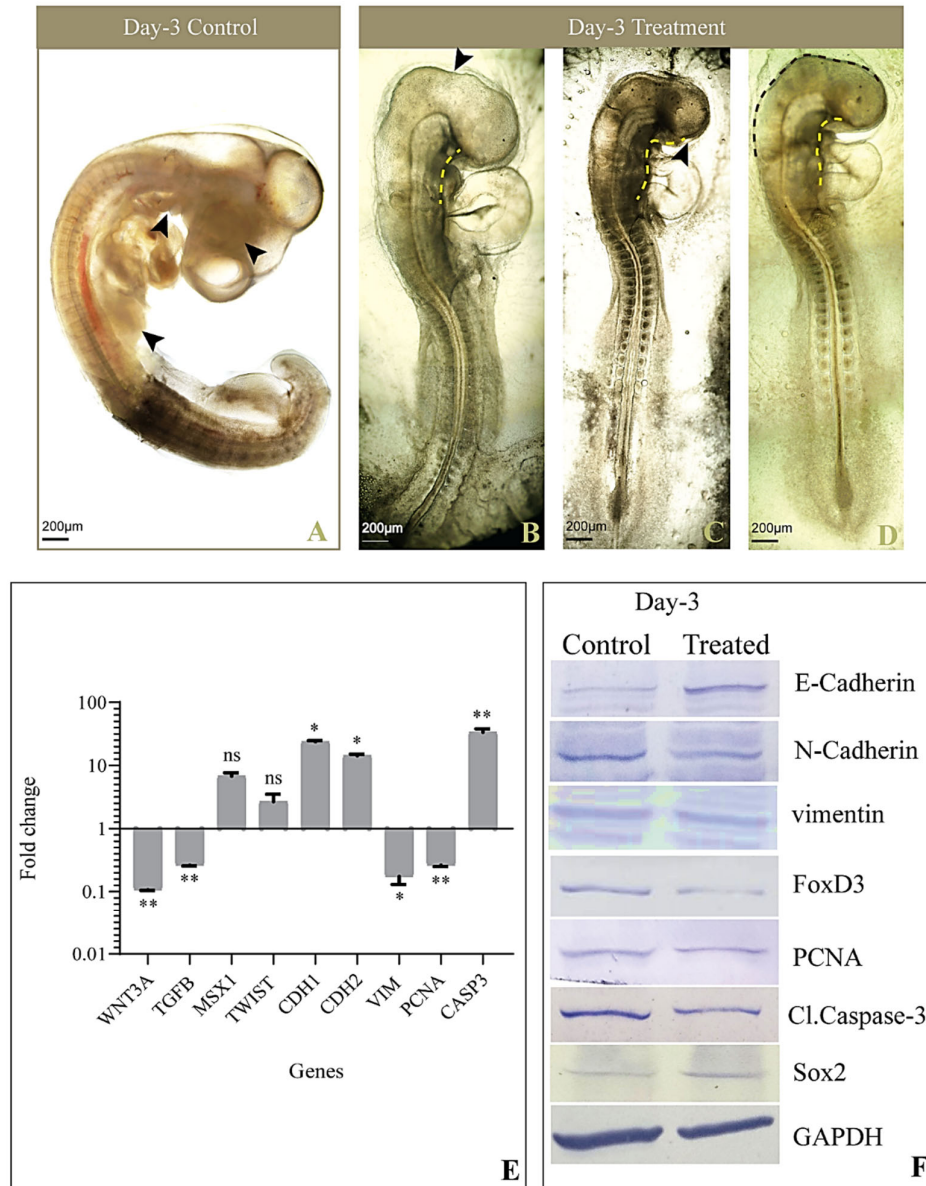


Figure 4. Morphological and molecular observations of Day-3 embryo after treatment. (A) Control embryo showing a completely developed forebrain, midbrain and hindbrain, visceral clefts, limb buds, and a primitive eye (black arrowhead); (B) Treated embryo indicating poorly developed brain regions (black arrowheads), the absence of a visceral cleft (yellow dotted line), and limb buds; (C) Day-3 etoricoxib-treated embryo showing the absence of distinct brain regions, abnormal curving of the body, visceral clefts not formed (yellow dotted line), and the absence of a primitive eye (black arrowhead); (D) Etoricoxib-treated embryo showing an abnormal visceral cleft (yellow dotted line), and the head region is defectively formed (brown dotted line); (E) Transcript level of genes regulating head formation and neural crest cell migration in the etoricoxib-treated Day-3 embryo. Values are expressed as fold change (mean ± SEM). Fold change values of treated embryo are compared with respective controls for all the genes (ns: non-significant, *: $p \leq 0.05$, **: $p \leq 0.01$); (F)

Western blot image showing the comparative expression of E-cadherin, N-cadherin, FoxD3, vimentin, PCNA, Caspase-3, and Sox2 on Day-3. GAPDH was taken as the loading control (n = 3 with 30 eggs per group).

3.3. Histological Observations

The extent of hindrance in the migration of cranial neural crest cells upon COX-2 inhibition was studied by the differential staining of Day-2 chick embryos using hematoxylin and eosin stains. The control embryos showed well-formed CNCCs, migrating toward the dorsal side of the neural tube, and a perfectly formed sclerotome (Figure 5A). In contrast, treated embryos showed sparsely distributed CNCCs, indicating delayed formation and migration. The architecture of the sclerotome was also found improper (Figure 5B).

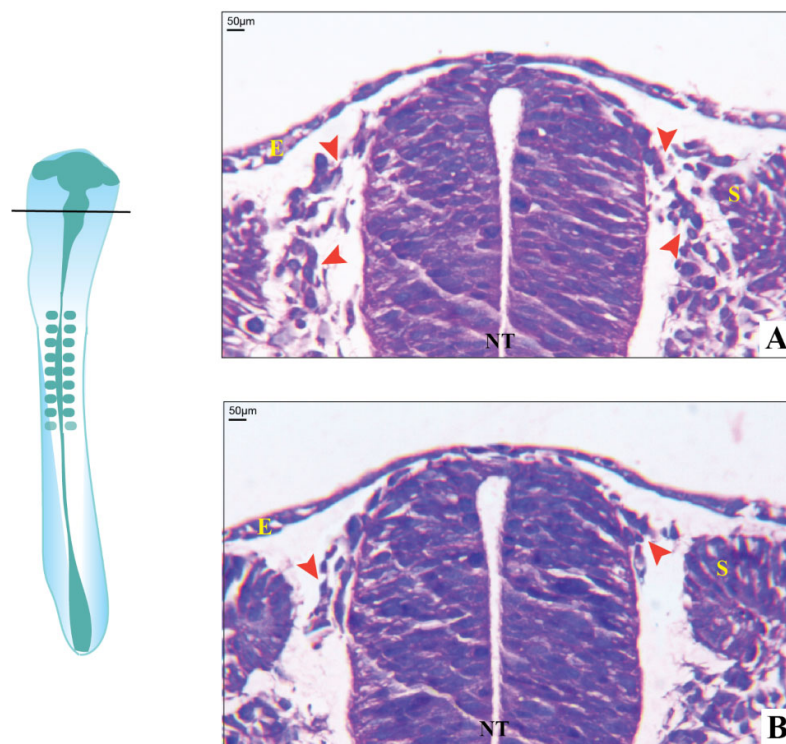


Figure 5. Histology of chick embryos in the transverse section. (A) Day-2 control with well-developed neural crest cells migrating towards the ventral side of the neural tube (red arrowheads); (B) Day-2 etoricoxib-treated embryo, showing less number of neural crest cells formed along with delayed migration (red arrowheads) (where E—epithelium, NT—neural tube, and S—sclerotome).

3.4. Expression of Genes Involved in EMT and CNCC Migration.

As mentioned previously, during CNCC migration, Wnt/ β -catenin and TGF- β , along with their downstream molecules, play an important role in EMT, cell survival, and proliferation. Hence, the transcriptional status of WNT3A, TGF β , MSX1, TWIST, CDH1, CDH2, VIM, PCNA, and CASP3 was examined across all three days in the control and treated embryos. On Day-1, the treated embryos elicited a significant reduction in the expression of WNT3A, while TGF β transcripts reduced marginally compared to the control. Meanwhile, MSX1 showed a remarkable ten-fold increase in the treated embryos. TWIST transcripts increased negligibly in the treated embryos, along with a conspicuous increase

in the CDH1 gene expression on Day-1 compared to control embryos. A noticeable reduction in CDH2 and VIM gene expression was recorded in COX-2-inhibited embryos on Day-1. PCNA and CASP3 significantly decreased simultaneously (Figure 2F). On Day-2, the etoricoxib-treated embryos showed a remarkable reduction in the expression of the migration of specific genes, namely WNT3A, TGFB, MSX1, TWIST, CDH2, and VIM, whereas CDH1 and CASP3 transcripts increased significantly (Figure 3E). PCNA, a known cell proliferation marker, reduced noticeably on Day-2 compared to the control. Furthermore, on Day-3, the levels of WNT3A, TGFB, VIM, and PCNA transcripts decreased significantly, and MSX1 expression slightly increased in the treated embryos. TWIST showed a marginal elevation at this time, while a significant increase in the levels of CDH1, CDH2, and CASP3 was observed (Figure 4E).

3.5. Levels of Proteins Involved in EMT and CNCC Migration

The protein expression of key regulators of EMT, CNCC proliferation, apoptosis, and migration such as E-cadherin, N-cadherin, FoxD3, vimentin, PCNA, cleaved Caspase-3, and Sox2 was measured by Western blot, followed by a densitometric analysis of the bands. The results revealed a significant upregulation of E-cadherin in the treated embryos compared to the respective control embryos across all three stages studied (Figures 2G, 3F, and 4F). On Day-1, N-cadherin reduced significantly in the treated embryos, which also continued for the following stages (Days-2 and 3) compared to the control. FoxD3 protein expression was not detected on Day-1 in both control and treated embryos, while on Day-2, it reduced remarkably in the treatment group. Furthermore, on Day-3, the level of FoxD3 remained low in the treated embryos compared to the control (Figures 3F and 4F). Another crucial EMT regulator, namely vimentin, was not recorded in both control and treated Day-1 embryos, while the Day-2 treated embryos showed no visible alteration compared to the respective control. However, on Day-3, treated embryos expressed a slight reduction in their expression compared to the Day-3 control. Parallel analysis of PCNA revealed that, compared to the control, its expression remained unaltered on Day-1 (Figure 2G) and further plunged significantly at the following stages (Days-2 and 3) (Figures 3F and 4F). Cleaved Caspase 3, on the other hand, reduced marginally on Day 1 in the treated embryos, while its level significantly increased on Day-2 compared to the respective controls. On Day-3, its level elevated negligibly compared to the respective control. Further, Sox2 levels decreased on Day-1 and subsequently on Days-2 and 3 in the treated group of embryos compared to the respective controls.

4. Discussion

Cranial neural crest cells are the most important pool of progenitors and migrate and form various structures of the facial region such as frontonasal, maxillary, and mandibular prominence in developing embryos [23]. In order to understand the mechanisms underlying CNCC migration, which plays a crucial role in the early development of craniofacial structures, the avian model is found to be most suitable. It is closely related to mammals, and the migration pattern of CNCCs is identical and conserved in both these classes of chordates [24]. The factors responsible for CNCC migration are widely accepted to be conserved across various classes of vertebrates. One such factor is COX-2, a member of the cyclooxygenase family involved in cellular processes such as proliferation, migration, angiogenesis, and differentiation [14,15,25]. It is found to be present during the developmental period of the embryo, which regulates the sculpting of various organs [20]. It is conserved among vertebrate species, but its role in embryonic development is still not very well explored. In zebrafish, COX-2-derived PGE₂ promotes embryonic vasculature maturation [26,27]. These studies substantiate that COX-2 is involved in the governance of cellular and molecular processes required during the early development of embryos. Hence, in the current study, the involvement of COX-2 in craniofacial patterning was investigated by using its specific pharmacological inhibitor, etoricoxib.

The administration of etoricoxib hampered CNCC migration and survival, resulting in several downstream morphological defects such as incomplete head vesicle formation, the absence of an optic vesicle, and defective neural tube formation [28–31]. As all these are the effects of abnormal CNCC migration or insufficient CNCC survival, the present study focused on the expression patterns of underlying signaling molecules that contribute to craniofacial patterning via CNCC fate determination. A COX-2 activity assay was performed to confirm the inhibition triggered by etoricoxib addition. COX-2 is known to be localized at the region of the neural tube in developing embryos at Days 1–3 [20,32]. In the present results, a reduction in COX-2 activity also caused an alteration in the levels of major regulators of the CNCC migration pathways in the treatment group of embryos. The expression of TGF- β and Wnt3A, along with their downstream signaling factors TWIST, MSX1, Sox2, FoxD3, vimentin, CDH1, and CDH2, was found disturbed under COX-2 inhibition in the current work.

Buch and colleagues illustrated an alteration in Wnt/ β -catenin signaling under the inhibition of COX-2, which hampers the regeneration of the lizard tail [33]. The involvement of Wnt3A in the delamination of CNCC has been reported during the early embryogenesis of chicks [34,35]. In the current study, a significant reduction in the expression of WNT3A was noticed upon COX-2 inhibition. Its mRNA level decreased on Day 1 and continued to stoop across Days 2 and 3 in the etoricoxib-treated embryos compared to the respective controls (Figures 2F, 3E, and 4E). A decreased WNT3A would have led to a smaller number of CNCCs formed under etoricoxib treatment. Histology results showed that the CNCCs formed were disoriented and lesser in number compared to the control, hence proving the impact of reduced COX-2 activity on normal CNCC formation and migration during early development.

Wnt and TGF- β are known to cooperate in processes involved in EMT [36]. In this case, along with Wnt, TGF- β also showed an unstable trend in Day-1, Day-2, and Day-3 embryos treated with etoricoxib. The gene expression of TGF- β continuously reduced across all stages in the treated embryos. Sela-Donenfeld and Kalcheim reported that an alteration in TGF- β disturbs the migration pattern, as it plays a crucial role in the switching of cadherins during CNCC delamination [37]. MSX1 and TWIST, the downstream mediators of TGF- β , also showed an alteration in gene expression at all stages (Days 1–3) in the etoricoxib treatment group.

Among the downstream regulators of TGF- β , MSX1 controls cellular proliferation and differentiation during early embryonic development. It is highly expressed in CNCCs and plays an important role in regulating the EMT process during embryonic development [38]. In the current results, a significant increase in MSX1 gene expression on Day-1 was followed by a continuous reduction on Day-2 and 3, which substantiates the results obtained through histology. The CNCCs might have delaminated on Day-1 due to an elevation in MSX1 gene expression, although they could not survive or migrate to their destined locations under reduced COX-2 activity. Parallel to MSX1, TWIST gene expression also showed concomitant changes at the initial stages observed here, which further consolidates the idea of cell survival and cell turnover running concurrently to each other [39,40]. In normal conditions, a decline in the level of TWIST causes CNCC to reside in pharyngeal arches and acquire their fates at later stages of migration. In our study, the level of TWIST remained high even at later stages (until Day-3) under the influence of a COX-2 antagonist. This might have hampered the ability of CNCCs to proliferate and differentiate to form a well-organized cranial feature.

It is well established that epithelial cells undergo an EMT process when E-cadherin is repressed and the cell–cell adhesion is negatively affected. This further leads to cytoskeletal changes in the cells, thus allowing motility [13]. In addition, the loss of N-cadherin is known to cause an interruption in the directed migration phenotype in *Xenopus* neural crest cells [41]. On the other hand, EMT is a function of well-regulated levels of E-cadherin, N-cadherin, and vimentin [42–44]. A decline in CDH1 and an escalation in CDH2 levels lead to the initiation of EMT in the neural tube to form neural crest cells [45]. In the present

study compared with respective controls, embryos facing compromised COX-2 activity displayed an increase in E-cadherin both at the gene and protein levels, along with a subsequent reduction in vimentin and N-cadherin on Days-1 and 2, which visibly impeded both CNCC formation and migration. However, by Day-3, both CDH1 and CDH2 increased back to a similar level, which could be due to the compensatory nature of the embryo. Meanwhile, the gene and protein levels of vimentin remained low, even on the third day, indicating the disturbed EMT. This resulted in perturbed patterning of the head region, optic vesicle, and neural tube in the treated embryo.

Furthermore, the expression of FoxD3 was checked, as it is a pivotal marker of CNCCs, facilitating their survival [46,47]. It has been documented that FoxD3 regulates the expression of cell adhesion molecules such as E-cadherin and N-cadherin [48]. In the current study, its protein level expression was recorded from Day-2 onward in both the control and treatment groups. This reinforces the fact that FoxD3 expression only begins after the HH 8 stage in a developing chick embryo [49]. In the treated embryos, FoxD3 protein expression plunged on both Days-2 and 3 compared to the respective controls. This implies the deleterious effects of the drug on the CNCC titer and also its migration.

In order to comment on the cell proliferation in CNCCs, the PCNA transcript and proteins were checked and found to be significantly reduced across all three days in the treated embryos compared to control embryos. In accordance with these data, cleaved Caspase-3 also showed a major upregulation in gene and protein expression at the three stages in the treatment group. These results direct toward the derailed cell proliferation of the delaminated CNCC due to the lacking PCNA status, while an analogous rise in the level of Caspase triggers cell death instead. Overall, CNCCs are unavailable for the normal patterning of frontonasal prominence in the treated embryos due to the deleterious impact of perturbed COX-2 function. A pictorial overview of the result is presented in Figure 6.

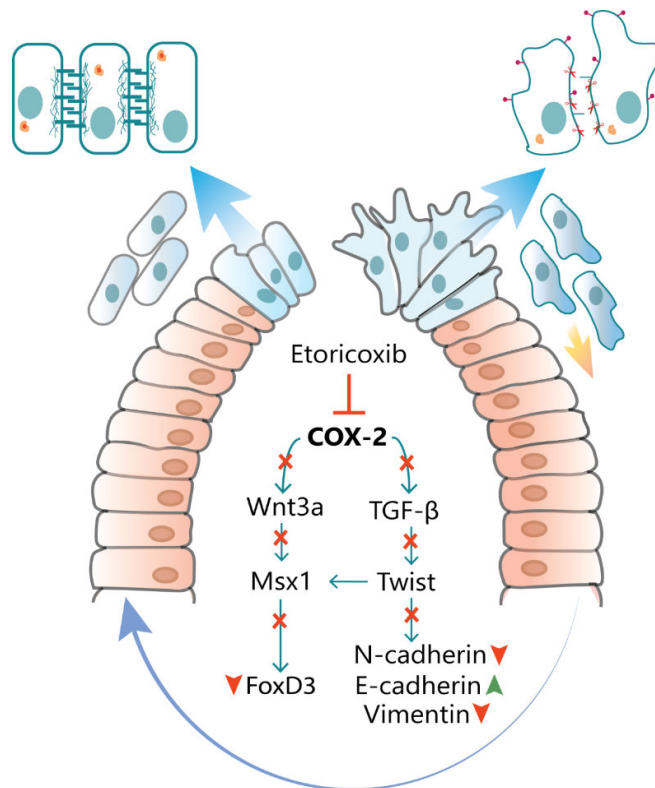


Figure 6. Expression pattern of genes downstream COX-2 upon etoricoxib treatment: a pictorial overview.

Based on our observations, it could be construed that COX-2, perhaps through its downstream effector PGE₂, regulates the temporal expression pattern of the factors responsible for CNCC formation, proliferation, and migration. Any alteration in the normal titer of COX-2 by accidental prenatal exposure to its commonly used pharmacological inhibitors would result in craniofacial dysmorphism, as observed in the current study due to dysregulation of cranial patterning.

Author Contributions: The work was conceived by S.B. Data acquisition and analysis were conducted by B.P. and U.V. The manuscript was drafted by B.P., U.V. and K.K. The draft was reviewed by D.D. and S.B. All authors have read and agreed to the published version of the manuscript.

Funding: This research did not receive any specific grant from any funding agencies.

Institutional Review Board Statement: The study was conducted according to the guidelines of the Declaration of Helsinki, and approved by the Institutional Animal Ethics Committee (IAEC) Ref No. MSU-Z/IAEC/09-2020 of The Maharaja Sayajirao University of Baroda, Vadodara, as per the guidelines of Committee for the Purpose of Control and Supervision of Experiments on Animals (CPCSEA), Govt. of India. All the experiments were performed as per the ethical approval and protocols.

Informed Consent Statement: Not Applicable.

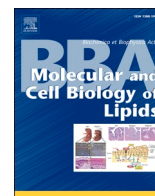
Data Availability Statement: The data presented in this study are available within the article.

Conflicts of Interest: The authors declare no conflicts of interest.

References

1. Fish, J.L. Developmental mechanisms underlying variation in craniofacial disease and evolution. *Dev. Biol.* **2016**, *415*, 188–197.
2. Suzuki, A.; Sangani, D.R.; Ansari, A.; Iwata, J. Molecular mechanisms of midfacial developmental defects. *Dev. Dyn.* **2016**, *245*, 276–293.
3. Snider, T.N.; Mishina, Y. Cranial neural crest cell contribution to craniofacial formation, pathology, and future directions in tissue engineering. *Birth Defects Res. Part C Embryo Today Rev.* **2014**, *102*, 324–332.
4. Alfandari, D.; Cousin, H.; Marsden, M. Mechanism of Xenopus cranial neural crest cell migration. *Cell Adhes. Migr.* **2010**, *4*, 553–560.
5. Trainor, P.A. Craniofacial birth defects: The role of neural crest cells in the etiology and pathogenesis of Treacher Collins syndrome and the potential for prevention. *Am. J. Med Genet. Part A* **2010**, *152*, 2984–2994.
6. Vaglia, J.L.; Hall, B.K. Patterns of migration and regulation of trunk neural crest cells in zebrafish (*Danio rerio*). *Int. J. Dev. Biol.* **2002**, *44*, 867–881.
7. Kulesa, P.; Ellies, D.L.; Trainor, P.A. Comparative analysis of neural crest cell death, migration, and function during vertebrate embryogenesis. *Dev. Dyn. An Off. Publ. Am. Assoc. Anat.* **2004**, *229*, 14–29.
8. Dorsky, R.I.; Moon, R.T.; Raible, D.W. Environmental signals and cell fate specification in premigratory neural crest. *Bioessays* **2000**, *22*, 708–716.
9. Wu, J.; Saint-Jeannet, J.P.; Klein, P.S. Wnt–frizzled signaling in neural crest formation. *Trends Neurosci.* **2003**, *26*, 40–45.
10. Basch, M.L.; Bronner-Fraser, M. Neural crest inducing signals. In *Neural Crest Induction and Differentiation*; Springer: Boston, MA, USA, 2006; pp. 24–31.
11. Ezin, A.M.; Fraser, S.E.; Bronner-Fraser, M. Fate map and morphogenesis of presumptive neural crest and dorsal neural tube. *Dev. Biol.* **2009**, *330*, 221–236.
12. Gilbert, S.F. The morphogenesis of evolutionary developmental biology. *Int. J. Dev. Biol.* **2003**, *47*, 467–477.
13. Yang, J.; Weinberg, R.A. Epithelial-mesenchymal transition: At the crossroads of development and tumor metastasis. *Dev. Cell* **2008**, *14*, 818–829.
14. Ricciotti, E.; FitzGerald, G.A. Prostaglandins and inflammation. *Arterioscler. Thromb. Vasc. Biol.* **2011**, *31*, 986–1000.
15. Wu, G.; Luo, J.; Rana, J.S.; Laham, R.; Sellke, F.W.; Li, J. Involvement of COX-2 in VEGF-induced angiogenesis via P38 and JNK pathways in vascular endothelial cells. *Cardiovasc. Res.* **2006**, *69*, 512–519.
16. Sharma, P.; Suresh, B. Influence of COX-2-Induced PGE₂ on the Initiation and Progression of Tail Regeneration in Northern House Gecko, *Hemidactylus flaviviridis*. *Folia Biol.* **2008**, *54*, 193–201.
17. Jana, S.; Chatterjee, K.; Ray, A.K.; DasMahapatra, P.; Swarnakar, S. Regulation of matrix metalloproteinase-2 activity by COX-2-PGE₂-pAKT axis promotes angiogenesis in endometriosis. *PLoS ONE.* **2016**, *11*, e0163540.
18. Jang, T.J.; Jeon, K.H.; Jung, K.H. Cyclooxygenase-2 expression is related to the epithelial-to-mesenchymal transition in human colon cancers. *Yonsei Med. J.* **2009**, *50*, 818–824.
19. Neil, J.R.; Johnson, K.M.; Nemenoff, R.A.; Schiemann, W.P. COX-2 inactivates Smad signaling and enhances EMT stimulated by TGF- β through a PGE₂ dependent mechanisms. *Carcinogenesis* **2008**, *29*, 2227–2235.

20. Verma, U.; Gautam, M.; Parmar, B.; Khaire, K.; Wishart, D.S.; Balakrishnan, S. New insights into the obligatory nature of cyclooxygenase-2 and PGE₂ during early chick embryogenesis. *Biochim. Biophys. Acta BBA Mol. Cell Biol. Lipids* **2021**, *1866*, 158889.
21. Parsad, R. Some Statistical Techniques for Bio-efficacy Trials. *Indian J. Agric. Sci.* **2010**, *16*, 62–76.
22. Livak, K.J.; Schmittgen, T.D. Analysis of relative gene expression data using real-time quantitative PCR and the 2⁻ΔΔCT method. *Methods* **2001**, *25*, 402–408.
23. Santagati, F.; Rijli, F.M. Cranial neural crest and the building of the vertebrate head. *Nat. Rev. Neurosci.* **2003**, *4*, 806–818.
24. Stern, C.D. The chick: A great model system becomes even greater. *Dev. Cell* **2005**, *8*, 9–17.
25. Evans, C.B.; Pillai, S.; Goldyne, M.E. Endogenous prostaglandin E₂ modulates calcium-induced differentiation in human skin keratinocytes. *Prostaglandins Leukot. Essent. Fat. Acids* **1993**, *49*, 777–781.
26. Grosser, T.; Yusuff, S.; Cheskis, E.; Pack, M.A.; FitzGerald, G.A. Developmental expression of functional cyclooxygenases in zebrafish. *Proc. Natl. Acad. Sci. USA* **2002**, *99*, 8418–8423.
27. Ugwuagbo, K.C.; Maiti, S.; Omar, A.; Hunter, S.; Nault, B.; Northam, C.; Majumder, M. Prostaglandin E₂ promotes embryonic vascular development and maturation in zebrafish. *Biol. Open* **2019**, *8*, bio039768.
28. Grocott, T.; Johnson, S.; Bailey, A.P.; Streit, A. Neural crest cells organize the eye via TGF-β and canonical Wnt signalling. *Nat. Commun.* **2011**, *2*, 265.
29. Beebe, D.C.; Coats, J.M. The lens organizes the anterior segment: Specification of neural crest cell differentiation in the avian eye. *Dev. Biol.* **2000**, *220*, 424–431.
30. Le Douarin, N.M.; Brito, J.M.; Creuzet, S. Role of the neural crest in face and brain development. *Brain Res. Rev.* **2007**, *55*, 237–247.
31. Graham, A.; Begbie, J.; McGonnell, I. Significance of the cranial neural crest. *Dev. Dyn. An Off. Publ. Am. Assoc. Anat.* **2004**, *229*, 5–13.
32. Geliflimine, E.N. The effects of meloxicam on neural tube development in the early stage of chick embryos. *Turk. Neurosurg.* **2010**, *20*, 111–116.
33. Buch, P.R.; Sarkate, P.; Uggini, G.K.; Desai, I.; Balakrishnan, S. Inhibition of cyclooxygenase-2 alters Wnt/β-catenin signaling in the regenerating tail of lizard *Hemidactylus flaviviridis*. *Tissue Eng. Regen. Med.* **2017**, *14*, 171–178.
34. Dorsky, R.I.; Moon, R.T.; Raible, D.W. Control of neural crest cell fate by the Wnt signalling pathway. *Nature* **1998**, *396*, 370–373.
35. Patthey, C.; Gunhaga, L.; Edlund, T. Early development of the central and peripheral nervous systems is coordinated by Wnt and BMP signals. *PLoS ONE* **2008**, *3*, e1625.
36. Yang, Y.M.; Yang, W.X. Epithelial-to-mesenchymal transition in the development of endometriosis. *Oncotarget* **2017**, *25*, 41679–41689.
37. Sela-Donenfeld, D.; Kalcheim, C. Regulation of the onset of neural crest migration by coordinated activity of BMP4 and Noggin in the dorsal neural tube. *Development* **1999**, *126*, 4749–4762.
38. Han, J.; Ishii, M.; Bringas, P., Jr.; Maas, R.L.; Maxson, R.E., Jr.; Chai, Y. Concerted action of Msx1 and Msx2 in regulating cranial neural crest cell differentiation during frontal bone development. *Mech. Dev.* **2007**, *124*, 729–745.
39. Satokata, I.; Maas, R. Msx1 deficient mice exhibit cleft palate and abnormalities of craniofacial and tooth development. *Nat. Genet.* **1994**, *6*, 348–356.
40. Soo, K.; O'Rourke, M.P.; Khoo, P.L.; Steiner, K.A.; Wong, N.; Behringer, R.R.; Tam, P.P. Twist function is required for the morphogenesis of the cephalic neural tube and the differentiation of the cranial neural crest cells in the mouse embryo. *Dev. Biol.* **2002**, *247*, 251–270.
41. Theveneau, E.; Marchant, L.; Kuriyama, S.; Gull, M.; Moepps, B.; Parsons, M.; Mayor, R. Collective chemotaxis requires contact-dependent cell polarity. *Dev. Cell* **2010**, *19*, 39–53.
42. Thiery, J.P.; Aclouque, H.; Huang, R.Y.; Nieto, M.A. Epithelial-mesenchymal transitions in development and disease. *Cell* **2009**, *139*, 871–890.
43. Mendez, M.G.; Kojima, S.I.; Goldman, R.D. Vimentin induces changes in cell shape, motility, and adhesion during the epithelial to mesenchymal transition. *FASEB J.* **2010**, *24*, 1838–1851.
44. Loh, C.Y.; Chai, J.Y.; Tang, T.F.; Wong, W.F.; Sethi, G.; Shanmugam, M.K.; Looi, C.Y. The E-cadherin and N-cadherin switch in epithelial-to-mesenchymal transition: Signaling, therapeutic implications, and challenges. *Cells* **2019**, *8*, 1118.
45. Scarpa, E.; Szabó, A.; Bibonne, A.; Theveneau, E.; Parsons, M.; Mayor, R. Cadherin switch during EMT in neural crest cells leads to contact inhibition of locomotion via repolarization of forces. *Dev. Cell* **2015**, *34*, 421–434.
46. Stewart, R.A.; Arduini, B.L.; Berghmans, S.; George, R.E.; Kanki, J.P.; Henion, P.D.; Look, A.T. Zebrafish foxd3 is selectively required for neural crest specification, migration and survival. *Dev. Biology* **2006**, *292*, 174–188.
47. Teng, L.; Mundell, N.A.; Frist, A.Y.; Wang, Q.; Labosky, P.A. Requirement for Foxd3 in the maintenance of neural crest progenitors. *Development* **2008**, *135*, 1615–1624.
48. Cheung, M.; Briscoe, J. Neural crest development is regulated by the transcription factor Sox9. *Development* **2003**, *130*, 5681–5693.
49. Kos, R.; Reedy, M.V.; Johnson, R.L.; Erickson, C.A. The winged-helix transcription factor FoxD3 is important for establishing the neural crest lineage and repressing melanogenesis in avian embryos. *Development* **2001**, *128*, 1467–1479.



New insights into the obligatory nature of cyclooxygenase-2 and PGE₂ during early chick embryogenesis

Urja Verma^a, Maheswor Gautam^b, Bhaval Parmar^a, Kashmira Khairi^a, David S. Wishart^{b,c}, Suresh Balakrishnan^{a,*}

^a Department of Zoology, Faculty of Science, The Maharaja Sayajirao University of Baroda, Gujarat 390 002, India

^b Department of Biological Sciences, University of Alberta, Edmonton, AB T6G 2E9, Canada

^c Department of Computing Science, University of Alberta, Edmonton, AB T6G 2E9, Canada

ARTICLE INFO

Keywords:

Cyclooxygenase
Embryogenesis
Prostaglandins
Lipids
Development

ABSTRACT

Temporal expression patterns and activity of two cyclooxygenase (COX-1 and COX-2) isoforms were analysed during early chick embryogenesis to evaluate their roles in development. COX-2 inhibition with etoricoxib resulted in significant structural anomalies such as anophthalmia (born without one or both eyes), phocomelia (underdeveloped or truncated limbs), and gastroschisis (an opening in the abdominal wall), indicating its significance in embryogenesis. Furthermore, the levels of PGE₂, PGD₂, PGF_{2α}, and TXB₂ were assessed using quantitative LC-MS/MS to identify which effector prostanoid (s) had their synthesis initiated by COX-2. COX-2 inhibition was only shown to reduce the level of PGE₂ significantly, and hence it could be inferred that the later could be largely under the regulation of activated COX-2 in chick embryos. The compensatory increase in the activity of COX-1 observed in the etoricoxib-treated group helped to maintain the levels of PGD₂, PGF_{2α}, and TXB₂. Though the roles of these three prostanoids in embryogenesis need to be further clarified, it appears that their contribution to the observed developmental anomalies is minimal. This study has shown that COX-2 is functionally active during chick embryogenesis, and it plays a central role in the structural configuration of several organs and tissues through its downstream effector molecule PGE₂.

1. Introduction

Cyclooxygenase enzymes, which exist in two isoforms (COX-1 and COX-2), convert arachidonic acid from the plasma membrane into various prostanoids such as prostaglandins (PGs) and thromboxanes (TXs) [1]. Typically, of these two isoforms, COX-2 is considered to be the inducible type, whereas COX-1 is considered as the constitutive one. Both these isoforms are stimulated during inflammation to initiate the production of prostanoids, whereupon specific prostanoids are produced with the help of tissue-specific prostaglandin synthases to perform particular functions regionally [1]. The roles of COX-2 and the derived prostanoids have been elucidated through the genetic modification and pharmacological inhibition of the enzyme [2,3]. The majority of investigations over the past decade have focused on the role of COX-2 in tumorigenesis, which has certainly helped in understanding the aetiology of several cancers [3,4]. On the contrary, only a handful of studies have explored the involvement of prostaglandins induced via COX-2 in embryogenesis and other developmental processes. Essentiality of COX-

2 in facilitating appendage regeneration via modulation of the expression of WNT, FGF, and MMP has been recently identified in reptiles [5,6]. COX-2 induced PGs are also known to be actively functioning for ovulation, fertilisation, decidualisation, and implantation in mammals [7,8]. More recently, COX-2 was found to interfere with blastocyst hatching, a prelude to successful implantation, in hamsters [9]. Additionally, Loftin and colleagues reported COX-2 to be necessary for the closure of ductus arteriosus in mice [2]. Likewise, the ubiquitous expression of COX-2 in early stages of embryonic development has been shown to result in skeletal deformities in a novel COX-2 transgenic mouse model [10]. In an effort to understand what tissues might be affected, Stanfield and colleagues (2002) localised COX-2 in rat embryonic, and foetal tissues, wherein its presence was found in the heart, kidney, skin, and cartilage [11]. These studies indeed suggest that COX-2, either through its inhibition or activation, could have an effect on the development of a number of organs, organ systems or tissues in vertebrates.

In the present study, we ascertained the expression of COX-2 in the

* Corresponding author.

E-mail address: b.suresh-zoo@msubaroda.ac.in (S. Balakrishnan).

<https://doi.org/10.1016/j.bbalip.2021.158889>

Received 23 October 2020; Received in revised form 7 January 2021; Accepted 13 January 2021

Available online 15 January 2021

1388-1981/© 2021 Elsevier B.V. All rights reserved.

chick embryos during the first ten days of development by measuring its mRNA levels, protein levels, and enzymatic activity. Chick embryos do not show inflammation until after three weeks of development [12], and thus this model is ideal for studying the non-inflammatory roles of COX-2. After ascertaining its normal basal level, the activity of COX-2 was inhibited to understand its plausible roles in organ and limb formation. At the same time, we attempted to identify which prostanoid was most significantly affected in response to COX-2 inhibition and to ascertain its role in embryogenesis. The status of COX-1 in the same tissues was also assessed. Further, the compensatory behaviour of COX-1 for the temporally regulated functions was studied in detail. Overall, this study focussed on the functional status of COX-2, its downstream effector PGE₂, and its plausible roles during embryogenesis.

2. Material and methods

2.1. Animals/egg procurement and ethical statement

Experiments involving embryos were carried out in accordance with the guidelines of the Committee for the Purpose of Control and Supervision of Experiments on Animals (CPCSEA), protocols were approved by Institutional Animal Ethics Committee (IAEC; No. MSU-Z/IAEC/05-2019). Eggs from Rhode Island Red (RIR) chickens (*Gallus domesticus*) were obtained from the intensive unit of the government poultry farm in Vadodara, Gujarat, India. Eggs were candled for marking air cells and wiped with a povidone-iodine solution before any treatment and incubation.

2.2. Experimental design

Eggs were randomly divided into control and treatment groups. Of which, control groups were treated (via syringe) with 50 µl of Milli-Q water, while treatment group eggs were administered with the same volume of 70 µg/ml (LOEC) of etoricoxib prepared by sonicating the compound-Milli-Q water mixture for 2 h. Each treated egg, therefore, received 3.5 µg of etoricoxib in a solution form. This etoricoxib solution was used for all the experiments other than the dose range study. The eggs were treated with the same concentration of etoricoxib at the intervals of three days as decided based on the COX-2 activity study (as discussed in Results). Post-treatment, eggs were incubated at 37 ± 0.5 °C and 67 ± 2% relative humidity inside a sterile form environment chamber (ThermoFisher Scientific, USA) until the isolation day, depending upon the experiment.

2.3. Dose range and morphometry

Pharmaceutical grade etoricoxib was received as a gift from Sun Pharma Advanced Research Company, Vadodara. Aqueous suspensions of etoricoxib at concentrations of 10, 50, 100, 150, 200, 250, 300, 350, 400, 450, and 500 µg/ml. A 50 µl dose was administered into an air cell using an insulin syringe. Eggs were incubated until day-10 (HH36), and embryos were checked for mortality and/or deformities. A total of 30 eggs were taken as the control group and 50 for each treatment group to circumvent treatment-induced variance. Control correction for such varied sample sizes amongst groups can be done by the Sun-Shepard's formula [13]. Corrected mortality was subtracted from 100, which yielded the % survival in various treatment groups. These data were used for non-linear fit analysis, with the LD₅₀ being calculated using GraphPad PRISM software (GraphPad Software Inc., USA). Analysis of Variance (ANOVA) followed by Dunnett's multiple comparison (post-hoc) test was performed for comparison of means (with 95% confidence interval) of all the groups with that of control survival rate. At this stage, deformities were observed and noted for their occurrence rates. The observed malformations were divided into four classes to identify the most frequent ones. All the head, eye, and beak related deformities were classified under craniofacial deformities. Varied limb lengths and web

defects were classified under limb deformities. Embryos possessing omphalocele or gastroschisis were placed under the visceral deformities class. Embryos exhibiting haemorrhages were classified separately. Sample sizes were 30 eggs for control and 50 for treated in each of the three replicates of this experiment.

2.4. COX-2 immunostaining

Embryos at days 1 and 2 (control group) were isolated with the help of a modified filter ring method [14]. The obtained embryos were fixed with pre-chilled methanol, mounted on a clean slide coated with albumen, and immunostained with a monoclonal primary COX-2 antibody according to the manufacturer's guideline (Abcam immunostaining protocols). Briefly, the slides were submerged three times in wash buffer (TBST – tris 24 g, NaCl 88 g, 1-l Milli-Q water; pH 7.6) for 15 min. The slides were incubated with a blocking buffer (2% BSA prepared in TBST) for 1 h. They were then placed in the primary antibody-filled coupling jar for 4 h at room temperature. The excess primary antibody was removed using three subsequent washes with wash buffer. Next, they were incubated in secondary antibody for 1 h at room temperature. The excess of the secondary antibody was removed with the help of three washes. After this step, the streptavidin and substrate were added in two different steps with the washing step in between. Water was added as soon as the colour developed. The same methodology was applied to the deparaffinised sections of days 3 to 10 embryos pre-mounted on slides, wherein deparaffinisation was carried out using two xylene dips for 15 min before other part of methodology. Sections were rehydrated by submerging the slides in 100%, 95%, 70%, and 50% ethanol gradients for 5 min each. The dilution used both for primary and secondary antibody was 1: 1000. Anti-COX-2 antibody (Sigma-Aldrich, USA, SAB4200576) and biotinylated 2° anti-rabbit IgG antibodies were diluted with assay buffer (diluted 1:200 in assay buffer – 500 mM tris-HCl; 1500 mM NaCl; 2% BSA; 0.02% Sodium Azide). Photographs were taken using Catcam eyepiece camera and Catymage software mounted on a light microscope.

2.5. Quantitative real-time PCR

The standard TRIzol method was used to isolate total RNA from embryos isolated at each day from days 1 to 10 of development, as per the manufacturer's guideline (Applied Biosystems, USA). Three embryos were pooled from each stage for each of the three replicates of this experiment. Fluorescence-based qubit assay was used according to the manufacturer's protocol (ThermoFisher Scientific, USA) to check RNA quantities. Complementary DNA was prepared from 1 µg RNA using one step cDNA synthesis kit (Applied Biosystems, USA). The reaction was performed in a LightCycler96 (Roche Diagnostics, Switzerland) using SYBR green master mix. After initial denaturation at 95 °C, 32 cycles consisting of 95 °C, 60 °C, and 72 °C were set for 10 s each step. The internal standard was 18srRNA for this experiment. Using the Cq values, ΔCq was calculated for each day sample for each gene COX-1 and COX-2 using the methodology described by Livak and Schmittgen (2001) [15]. The initial numbers of fragments of COX-1 and COX-2 in various cDNA samples were interpolated using these ΔCq values from a standard graph. The primer sequences are mentioned in Table 1.

2.6. Western blot

Total protein was isolated by homogenisation of three embryos per stage by placing them in a lysis buffer with a protease inhibitor (P8340, Sigma-Aldrich, USA) and grinding the tissue with cold mortar-pestles. Bradford's method of quantification was used to quantify all isolated proteins [16]. Proteins were resolved on PAGE (Polyacrylamide Gel Electrophoresis) consisting of 12% resolving and 4% stacking gels. The semi-dry method of transfer was used to transfer the gel-separated proteins onto the PVDF membrane. The membrane was

Table 1

Primer sequences as obtained from NCBI.

Gene name	Forward primer	Reverse primer	NCBI ref id	Product length
COX-1	CGGAGTGCCTATCGCC	CACGGTTAACGGTGCC	XM_425326.5	133
COX-2	AACACAAGTGCCTACTCCG	CTGGTCCTTTGCGGTGATCT	NM_001167718.1	86
18s rRNA	GGCCGTTCTTAGTTGGTGA	TCAATCTCGGGTGGCTGAAC	NR_003278.3	144

immunostained for COX-1, and COX-2 using primary antibodies (Sigma-Aldrich, USA, MAB5586 for COX-1, SAB4200576 for COX-2) diluted 500 times in assay buffer (diluted 1:200 in assay buffer – 500 mM tris-HCl; 1500 mM NaCl; 2% BSA; 0.02% Sodium Azide). GAPDH (1:500 dilution, Sigma-Aldrich, USA) was used as an internal control. Biotinylated 2° polyclonal antibody of IgG type (Sigma-Aldrich, USA) was used. The previously described methodology was adopted for the performance and evaluation of western blot [17]. The original blot images were corrected for variations in the background by adjusting contrast. The protein sample used for COX-2 blot was used for GAPDH as well. The densitometric values are detailed in Supplementary Table 1.

2.7. COX activity assay

A kit-based assay was used to detect COX-1, COX-2, and total COX activity in both the control as well as treated samples from days 1 to 10 (Cayman Chemical, USA). The negative control, standards, controls, and treatment samples were assayed as per the manufacturer's description. Briefly, the embryos were rinsed with tris buffer (pH 7.4) to remove the red blood cells and were added in the pre-chilled buffer (0.1 M tris-HCl, pH 7.8, 1 mM EDTA). These were homogenised, and supernatant was collected after centrifugation at 8000g for 20 min at 4 °C. The supernatant was filtered using the nitrocellulose membrane filter and was immediately used for the assay. The assay was done with background wells (with inactivated boiled sample supernatants for each sample), standard wells (as provided with kits), sample wells (40 µl sample), and inhibitor wells (COX-1 inhibitor wells for calculating COX-2 activity and vice-versa for COX-1). A selective COX-1 inhibitor SC-560 and COX-2 inhibitor DuP-697 were used for the inhibitor wells. All the wells contained the assay buffer and haem along with the subject material (any one of the inactivated samples, standard sample, or inhibitor and sample). The plate was then incubated for 10 min at room temperature and added with 20 µl colourimetric substrate. Lastly, arachidonic acid (20 µl) was added to the wells and incubated for 10 min at room temperature. The absorbance was measured at 590 nm, which is the colourimetric absorbance of oxidised *N,N,N',N'*-tetramethyl-*p*-phenyldiamine (TMPD) corresponding to the amount of peroxidase activity of COX enzymes and therefore the amount of COX enzymes in the samples. Specific activities were calculated by dividing total protein values derived from Bradford assay. Multiple *t*-test was performed to determine the significant values between control and treatment groups of each COX isozymes and total COX. The means of COX-1 and COX-2 activities were also compared using the same test from the data obtained after three technical and six biological replicates.

2.8. LC-MS of etoricoxib

The presence of etoricoxib in treated samples and its endogenous absence in control samples was determined by liquid chromatography-mass spectrometry (LC-MS). Thirty embryos per group (control and treatment) were collected and pooled for methanol extraction. Samples were homogenised using a pre-chilled mortar and pestle in 90 µl cold methanol per mg of wet tissue weight. The homogenate was vortexed for 1 min, followed by sonication for 5 min. The liquefied homogenate was then centrifuged for 7 min at 12000g at 4 °C. The supernatant was collected and filtered via 0.4 µm filters. These samples were kept at –80 °C until used. For the liquid chromatography separation, a Thermo Fisher Scientific Synchronis C-18 column was used (250 mm × 4.6 mm, 5

µm particle size), the mobile phase was acetonitrile-water (90:10). The flow rate was 0.3 ml/min, with an injection volume of 15 µl. The standard solution was prepared with 70 µg/ml etoricoxib and was vortexed, sonicated, as well as centrifuged similarly to that of the samples to mitigate any technical errors. The Thermo Scientific Surveyor LC-system was coupled to a Thermo Icq fleet ion trap mass spectrometer operating in the positive ion mode. The instrument parameters were temperature, 270 °C; ion spray voltage, 5000 V; sheath gas pressure, 50 arb; and auxiliary gas pressure, 30 arb. Data were analysed on the xcalibur™.

2.9. PGE₂ concentration assay

Quantification of PGE₂ was carried out using a sandwich ELISA kit as per the manufacturer's suggestions (R&D Lab Systems, USA). Embryos were weighed, and about a gram of embryos per stage (of days 1 to 10) were homogenised in a pre-chilled mortar-pestle. The homogenates were centrifuged at 2000 ×g for 15 min to generate a clear supernatant. 1 ml of the supernatant was used for the PGE₂ assay. Concentrations were derived using the four-parameter algorithm graph (GraphPad Software Inc., USA) following the manufacturer's instructions. The experiment was repeated thrice. The statistical significance was derived with the help of two-way ANOVA, followed by Bonferroni's multiple comparison post-hoc test. The details of test parameters and values are included with the supplementary data (Supplementary Table 3).

2.10. LC-MS/MS of prostanoids

The chemicals used for this experiment were purchased from Cayman Chemicals. Commercial Prostaglandin D₂ (12010), Prostaglandin E₂ (14010), Prostaglandin F_{2α} (10007275), and Thromboxane B₂ (19030) were used as reference standard compounds. Prostaglandin F_{2α}-d₄ (10007275) was used as an internal standard for quantification and calibration, given the close structural similarities of the other prostanoids. For sample preparation, about 30 day-2 embryos were collected and placed in methanol (1 ml per gram of tissue) and ground using pre-chilled mortar-pestles. The homogenised tissue samples were then spiked with a 10 µg/l internal standard (ISTD). Vials were vortexed briefly and ultrasonicated for 5 min at room temperature. The samples were then shaken gently and centrifuged at 10000 ×g for 15 min at 4 °C. The supernatant was collected and stored at –80 °C until analysis. The samples were transported to the University of Alberta in tightly sealed vials at room temperature for LC-MS/MS analysis. Further standardisation of methodology used for isolation of the peaks of closely related compounds – the prostanoids was carried out at the University of Alberta.

An LC-MS system consisting of Agilent 1290 series UHPLC coupled to a Sciex QTRAP® 5500 mass spectrometer was used for the LC-MS/MS analysis. The system was controlled by the Sciex Analyst® 1.6.2 LC-MS software. An Agilent UHPLC system equipped with a Zorbax Eclipse XDB C18 analytical reverse-phase column (3.0 mm × 100 mm, 3.5 µm particle size, 80 Å pore size), connected to a Phenomenex (Torrance) SecurityGuard C18 pre-column (4.0 mm × 3.0 mm) was used for the chromatographic separation. The following conditions were used for the chromatographic separation: mobile phase A: 0.1% acetic acid in water; mobile phase B: Acetonitrile/isopropanol (90 / 10) with a gradient profile as: *t* = 0 min, 38% B; *t* = 3.5 min, 60% B; *t* = 4.25 min, 77.5% B; *t* = 6.25 min, 95% B; *t* = 9.0 min, 95% B; *t* = 9.1 min, 38% B; *t* = 11.6 min, 38% B; with a flow rate of 0.3 ml/min and injection volume

of 10 μ l. The column temperature was set at 40 °C. The mass spectrometric analyses were done in the negative ionisation mode with multiple reaction monitoring (MRM). The instrument parameters used for the analyses were: Curtain gas, 30 psi; CAD, medium; Temperature (TEM), 500 °C; ion source gas 1 (GS1), 50; ion source gas 2 (GS2), 50; ion spray voltage -4500 V. The Entrance Potential (EP) and Cell Exit Potential (CXP) were set at -10 V and -15 V for all the analytes, respectively. Collision energy (CE) and Declustering potential (DP) for each analyte were optimised by manual tuning. The CE and DP for the ISTD were the same as for PGF_{2 α} . The compound-dependent MS parameters used were as outlined in Supplementary Table 6. The calibration curve for each analyte was obtained by using a set of seven calibrants and an internal standard. Specifically, the concentrations of the calibrants were 25, 12.5, 6.25, 3.125, 1.56, 0.78, and 0.313 ng/ml. Calibration curves were obtained by plotting the ratio of analyte to ISTD response versus the calibrant concentration. Quadratic regression was used to fit the response by using 1/x weighting. Concentrations of samples were determined using the Analyst® 1.6.2 LC-MS software.

3. Results

3.1. COX-2 is expressed constitutively during embryogenesis and is inducible

COX-2 protein levels showed remarkable variation during the first ten days of chick embryonic development. Immunostained blot images showed that the COX-2 protein was present maximally during the first few days of development, while COX-1 was slightly higher at day-1 than its concentration at other stages (Fig. 1). Further analysis of the representative blot images revealed that the level of COX-2 protein reaches its maximum on day-1 of development, followed by a steady decline in the levels of COX-2 until day-4. After this, the levels of COX-2 protein increased slowly until day-10 (Fig. 1A). Levels of COX-1 protein remained more or less constant in all the stages except for day-1 in the control chick embryos (Fig. 1A). In comparison to its protein levels (Fig. 1A), the transcripts of COX-2 remained steady throughout the same period and did not show significant fluctuation until day-9 (Fig. 1A). Similarly, COX-1 gene expression was found to remain unchanged from days 1 to 10 of development (Fig. 1B).

In order to understand the spatial distribution of COX-2 in the developing chick embryo, immunolocalisation of COX-2 protein was performed in embryos from days 1 to 10 of development. As seen in Fig. 2A, COX-2 was present diffusely throughout the whole of the

embryo on day-1, with a more prominent presence evident in somites and optic vesicles. Over the following days, the distribution of COX-2 became even more circumscribed. On day-2, it became restricted to the areas surrounding the somites and the tubular heart (Fig. 2B). By day-3, COX-2 became particularly concentrated towards the cephalic field and surrounding the allantoic vesicle (Fig. 2C), and in the walls of atria and ventricles on day-4 (Fig. 2D), and limbs by day-5 (Fig. 2E & F). By day-6, the early cells of embryonic kidneys showed the presence of COX-2 in their cell membranes (Fig. 2G). COX-2 was also found at the distal end of the embryonic tail as well as in the somites (Fig. 2H). By day-7, the notochord showed the presence of COX-2, as seen in the transverse section of the same (Fig. 2I). COX-2 was detected in seminiferous tubule (Fig. 2J) by day-8 and in somites by day-9 (Fig. 2K & L). No immunoreactivity was observed in the antibody controls, which clearly demonstrated the absence of background noise (Supplementary Fig. 1). The temporal progression and presence of COX-2 in these regions suggest its possible role in early embryogenesis, especially in processes, such as cell migration, differentiation, or pattern formation.

3.2. Selective inhibition of COX-2 activity using etoricoxib led to stunted growth, structural anomalies, and mortality in the chick embryo

The presence of COX-2 from the very first day of chick development points to its possible regulatory role in the embryogenesis. To further assess this role, the activity of COX-2 was inhibited using etoricoxib, an isotype-specific pharmacological inhibitor, and the progression of development was followed for a period of 10 days. As a prelude, a dose-range study was conducted to select an appropriate treatment concentration of etoricoxib. The result revealed a dose-dependent increase in the mortality rate, wherein half of the embryos that received a concentration of 144 μ g/ml of etoricoxib were found dead (Fig. 3A; Supplementary Table 4). The lowest observed effect concentration (LOEC) of etoricoxib was computed to be 70 μ g/ml, at which the survival rate of malformed embryos was found to be 71%, which was significantly lower than the control survival rate (Supplementary Table 4, 5). Embryos subjected to this dose were isolated, and a targeted liquid chromatography-mass spectrometry (LC-MS) study was performed to detect and verify etoricoxib inclusion. The standard solution of etoricoxib showed that the pure compound eluted from the LC column at 6 min (Fig. 3B), as confirmed by the *m/z* peak of 359 (positive mode, molecular weight 358) (Fig. 3C). The same peak was observed in the treatment group eluting at the same timepoint as well (Fig. 3F & G). The control group, however, did not show the presence of this mass in any of

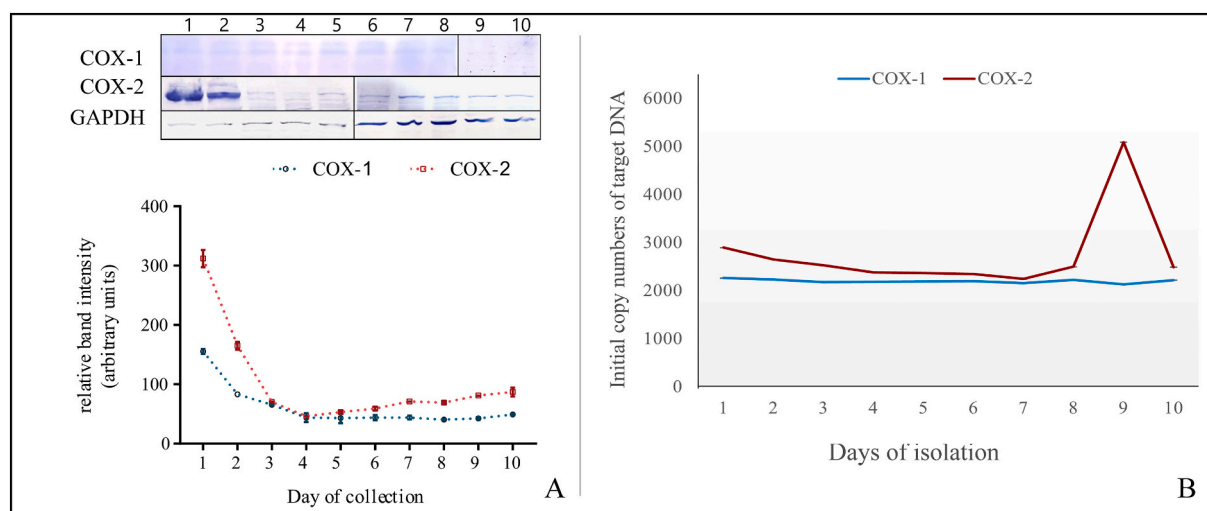


Fig. 1. Gene and protein expression levels of COX-1 and COX-2. A. Western blot images (upper panel), mean band intensity (in arbitrary unit) computed from blots (lower panel); B. The initial copy numbers of cDNA fragments of COX-1 and COX-2 as replicated using specific primers. $n = 3$.

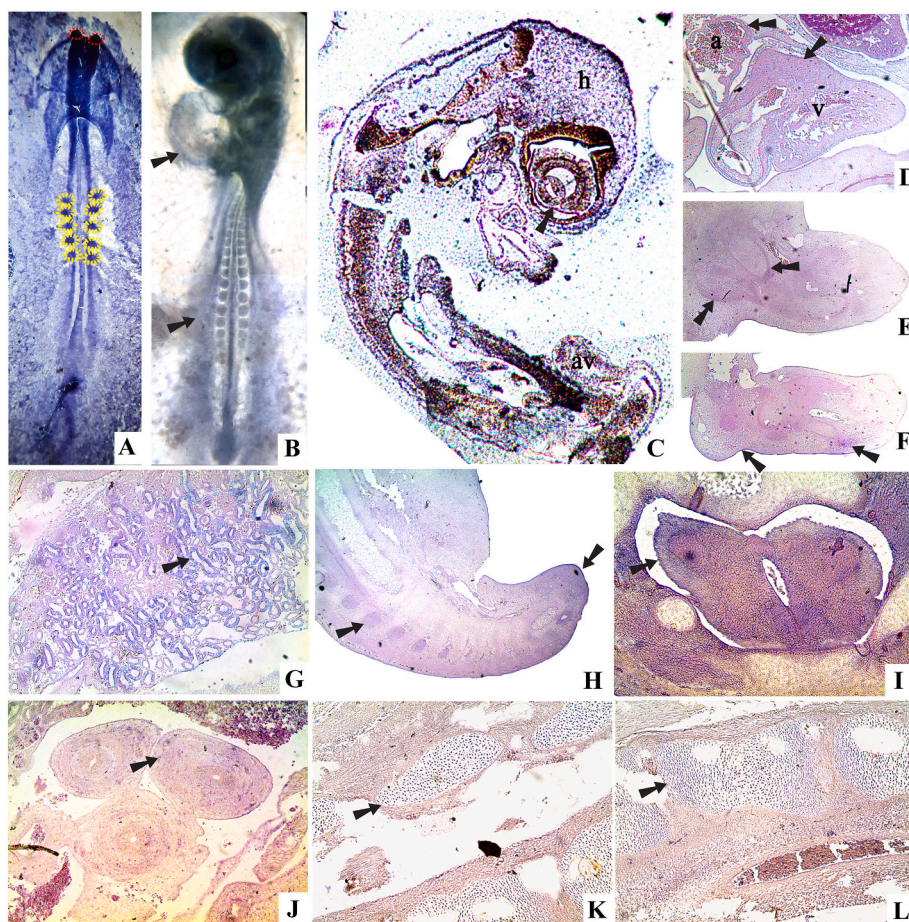


Fig. 2. Chick embryonic tissues immunostained for COX-2. A. whole mount of day-1 embryo, somites (yellow circles), optic vesicles (red circles); B. Day-2 embryo whole mount, developing tubular heart (black arrows); C. Day-3 embryo longitudinal section, head (h), allantoic vesicle (av); D. Day-4 embryonic heart longitudinal section, atria (a), ventricles (v); E. Sagittal section of forelimb of day-5, cartilage condensation areas shown with black arrows; F. Day-5 hindlimb sagittal section, the developing bones near cartilage condensation areas and in the epithelium of limb tissue (black arrows); G. Day-6 kidney transverse section; H. Day-6 embryo longitudinal section, somites and tail region pointed by black arrows; I. Transverse section of day-7 embryonic notochord; J. Day-8, Seminiferous vesicle (black arrow); K. Day-9, developing nerve cord (black arrow); L. Day-9, somites.

the peaks arising from 4 to 7 min of the LC run (Fig. 3D & E). The only peak seen in the control group was 243 m/z, which does not correspond to the etoricoxib peak.

Embryos treated with LOEC showed phocomelia (Fig. 4C), haemorrhages (Fig. 4C & G), anophthalmia (Fig. 4E), gastroschisis (Fig. 4B), omphalocele (Fig. 4D), abnormal body sizes (Fig. 4F), absence of feathers (Fig. 4F), and general developmental delay (Fig. 4F). The onset of limb development itself was delayed by the treatment with no limb buds seen in the 2-day embryos compared to the corresponding controls wherein limb buds are conspicuously visible (Fig. 4A). Broadly, COX-2 inhibition led to limb deformities (most commonly), followed by craniofacial and visceral deformities. The etoricoxib treatment also resulted in haemorrhage, albeit in relatively few (13%) embryos (Graphical abstract).

3.3. COX-1 compensates for the reduced activity of COX-2 under the influence of etoricoxib

To ascertain the possibility of compensatory upregulation of another COX isoform in response to COX-2 inhibition, 70 µg/ml etoricoxib (LOEC), was administered on day-0 of development and the activities of total COX, COX-1, as well as COX-2, were measured daily until day-10 of development. The result revealed that the overall activity of COX diminished significantly from day-1 until day-3 compared to the corresponding untreated controls (Supplementary Table 2). However, on day-4, significant recovery of total COX activity was observed in the treated embryos, indicating the appreciable clearance of etoricoxib. Based on the above observation, the eggs were treated with 70 µg/ml etoricoxib, on every third day of development, starting from day-0, then on days 3, 6, and 9. The same treatment regime was later used to understand which

COX isozyme showed a similar pattern of activity to that of total COX in the control group. Our results showed that the activity of COX-2 was modulated in tandem with that of the total COX activity throughout all stages of development in the control group. On the other hand, COX-1 activity was negligible at all the stages of development from days 1 to 10 in the control group. However, in the treatment group, when COX-2 activity was reduced, COX-1 activity increased (Fig. 5). Days 2, 6, and 9 corresponded to the days when COX-1 activity increased significantly as compared to its basal level in the control group. This strongly suggests the possibility of a compensatory regulation of the activity of COX-1 and COX-2 isozymes in chick embryogenesis.

3.4. PGE₂ concentration decreases concomitantly with COX-2 inhibition in chick embryonic tissues

Despite the apparent compensatory regulation of both COX isoforms, we hypothesised that the level of PGE₂, the ultimate product of the COX action, is maintained by COX-2 activity. To test this notion, the level of PGE₂ was measured using a commercial ELISA kit in both control and etoricoxib-treated embryos. The temporal trend seen in the tissue PGE₂ concentration was similar to that of COX-2 activity for most of the time points studied in both the control and the treated embryos (where the activity of COX-2 was significantly compromised). Although a compensatory increase in COX-1 activity was found in 2, 6, and 9-day old treated embryos, the PGE₂ concentration for these days showed only a marginal, statistically insignificant, increase compared to its basal level observed in the control embryos (Fig. 6). It is evident from this result that COX-1, even with its moderate increase in an activity, does not compensate for the reduced PGE₂ level in the etoricoxib-treated embryos. Therefore, PGE₂ levels seem to be under the regulation of

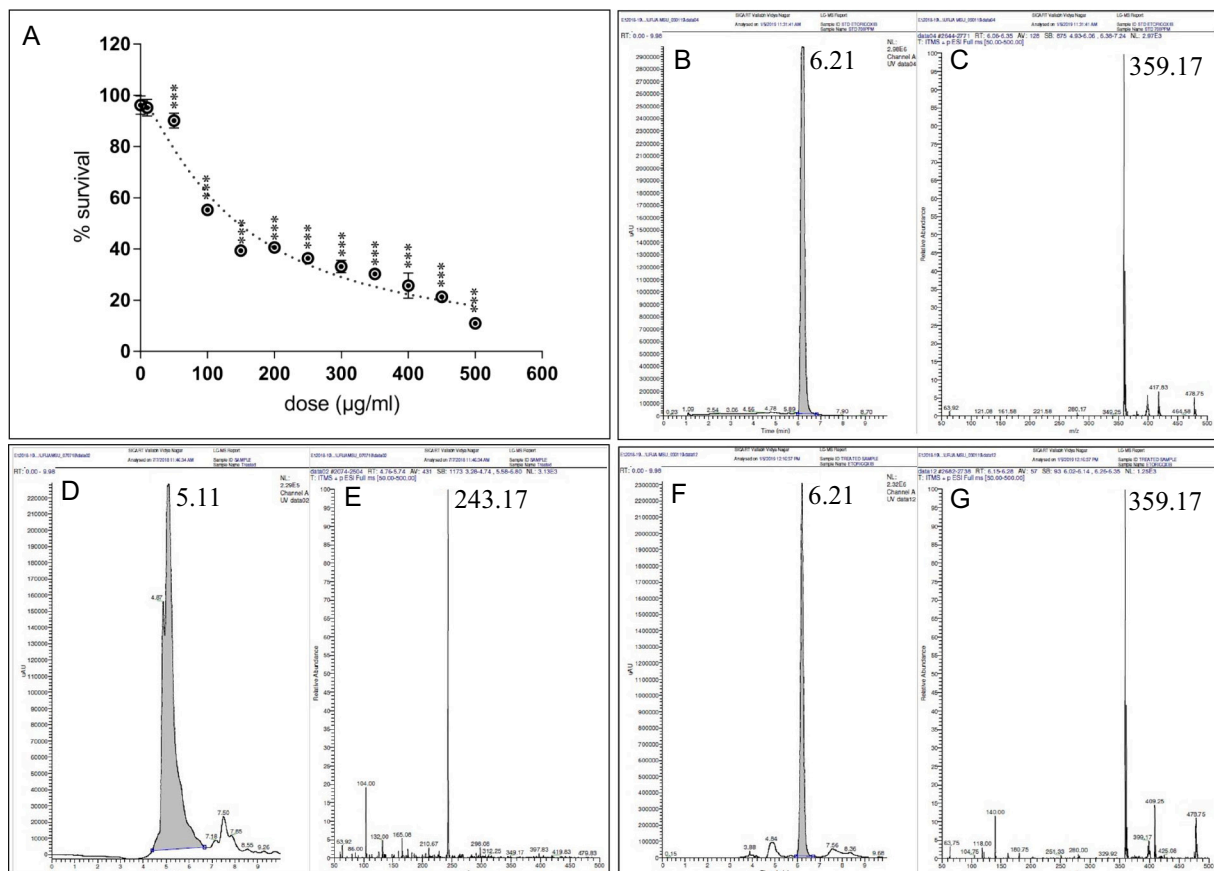


Fig. 3. A. Survival rates of embryos subjected to varying doses of etoricoxib. $n = 30$ for control group and $n = 50$ for treatment group, $***p \leq 0.001$; B: LC profile of a pure solution of etoricoxib (standard group); F: LC profile of the treated group; D: LC profile of the control group; C, E, and G represent the mass profiles of the compounds eluting at highlighted same timepoints in corresponding LC profiles B, D, and F respectively.

COX-2.

The above results were reaffirmed by measuring the levels of all four major prostanoids, namely PGE₂, PGD₂, PGF_{2 α} , and TXB₂ in control and treated embryos by employing reversed-phase UHPLC coupled to tandem mass spectrometry (LC-MS/MS). This experiment was performed on day-2 embryos. This was because at day-2 the activity of COX-2 was particularly high and the size of the embryos, compared to day-1 embryos, was sufficiently large to collect the biological material needed for the MS test (Figs. 1A & 4). Due to high levels of COX-2 expression, it was hypothesised that the prostanoid concentrations would also be elevated at this stage. We found that our developed LC-MS/MS method was able to efficiently separate and detect these prostanoids (Supplementary Fig. 2; Supplementary Table 6) and that optimum calibration curves could be calculated for each of these prostanoids to permit their accurate quantification. The LC-MS/MS method was further validated for its recovery performance, which further assured the accuracy of our quantifications (Supplementary Table 7).

Out of the four prostanoids measured by our LC-MS/MS assay, only the level of PGE₂ was found to be reduced significantly in the etoricoxib-treated embryos compared to untreated control embryos. In the control embryos, PGD₂ was found to have the highest concentration (18.13 ± 1.162 ng/g tissue weight), followed by TXB₂ at about half concentration of that of PGD₂ (Table 2). The level of PGE₂ dropped to half its control concentration (4.74 ± 0.257 ng/g tissue weight) in the treated group, which reached similar levels of the least concentrated prostanoid, PGF_{2 α} (2.86 ± 0.107 ng/g tissue weight) (Table 2). PGD₂, PGF_{2 α} , and TXB₂ did not show any significant changes between control and treated samples. PGI₂ was not detected in the embryos at this stage. Therefore, only PGE₂ was affected during embryonic COX-2 inhibition. This allows us to

conclude that PGE₂ is the effector molecule of COX-2 for pattern formation in these embryonic stages.

4. Discussion

Cyclooxygenase enzymes have been the subject of considerable research since they were first identified as the targets of many of the most popular and best-known anti-inflammatory drugs. Two COX isoforms (COX-1 and COX-2) have been identified and, in addition to their well-known roles in inflammation, they have also been found to participate in a plethora of other biological processes, ranging from ovulation and fertilisation to ageing and death [8,11]. One of the goals of this study has been to explore the role of COX-1 and COX-2 in embryogenesis. While a small handful of studies have been published, relatively few have looked at the differing roles of COX isotypes and the effects of their downstream effectors on the development of multiple organs and tissues. To explore this aspect more thoroughly, we systematically studied the temporal and spatial tissue expression of both COX-1 and COX-2, as well as their prostanoid by-products in early (1 to 10 days) chick embryos. We also correlated induced changes in COX-2 activity with detectable embryo defects.

In vertebrates, the COX-1 isozyme is constitutively expressed while COX-2 is an inducible isotype that responds to inflammatory signals. However, based on the results of the current study, COX-2 appears to be expressed constitutively during the course of normal chick embryogenesis. Our study has also revealed that the activity of COX-2 is unique for any given day of development and that this activity varied temporally in the embryonic tissues. This suggests a constitutive nature of this isoform. A clear temporal trend in COX-2 protein levels was seen in

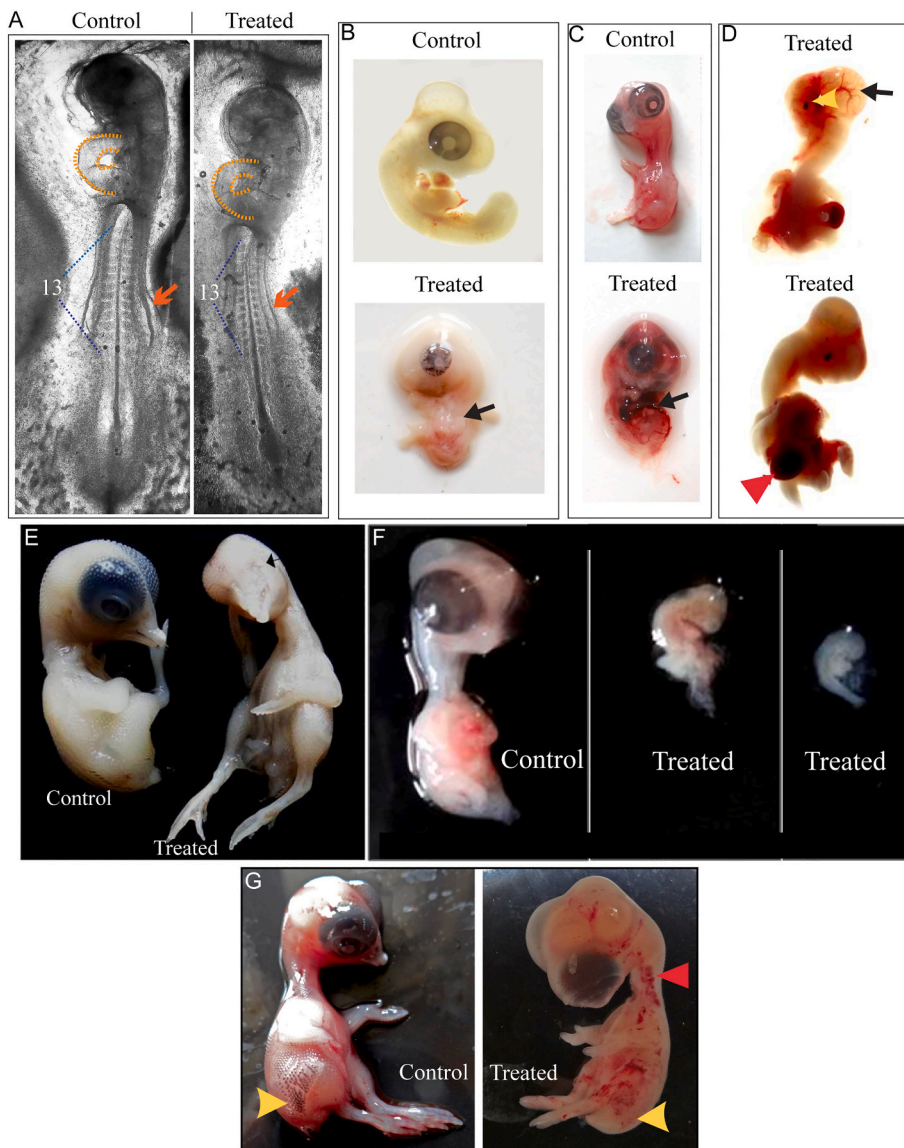


Fig. 4. Morphological anomalies caused by COX-2 inhibition. A. Day-2 embryos, absence of limb buds (orange arrow); B. Gastroschisis (black arrow) in day-5 treated embryos; C. Day-7 treated embryo with phocomelia along with severe haemorrhage (black arrow); D. Day-7 treated showing microphthalmia (yellow arrowhead), hydrocephalus (black arrow), and larger protruding heart (red arrowhead); E. Anophthalmia (black arrow) in treated day-10 embryo; F. Stunted growth in day-10 embryos; G. Absence of feathers in treated day-9 embryo (yellow arrows), Haemorrhage along the neck and other areas in treated embryos shown with a red arrowhead. $n = 50$ for each of the three technical replications.

embryos from day-1 till day-10 of their development when all the cellular events leading to organogenesis occur in chicks. It is noteworthy, that differing pattern in protein and transcript abundance as found in these timepoints, is typical of a protein that is not subject to induction at the level of gene expression [18]. Our result with chick embryos, however, contrasts with the data reported in mouse embryos, wherein organogenesis stages, i.e., gestational days 7 to 13, do not show the presence of COX-2 [11]. On the contrary, some reports suggest that COX-2 is required for ductus arteriosus closure and nephrogenesis in mice and rats [2,19,20].

Another key finding in this study is that experimental inhibition of COX-2 activity with etoricoxib can lead to multiple deformities in chick embryos. This reaffirms the role of COX-2 in organogenesis. Moreover, the inhibition of COX-2 caused anomalies of limbs and craniofacial structures of chick embryos, all of which were derived from cells localised with COX-2 on day-2 of development. Several other published studies have focussed on the roles of COX-2 in mice embryogenesis using knockout models. These studies found that some mouse embryos acquiesce in the absence of COX-2 gene and develop without showing patent ductus arteriosus [2,21]. The authors suggested the compensatory role of COX-1 might have allowed the embryos to survive without the ductus arteriosus closure defect. Therefore, the compensatory action

of COX-1 was checked in our chick embryo model by studying its activity along with that of COX-2, in both the control and etoricoxib-treated groups. COX-1 activity increased when the embryos were challenged with the COX-2 antagonist, etoricoxib, which partially compensated for the total cyclooxygenase activity until day-3. However, day-4 experimental embryos experienced a partial revival of COX-2 activity. This kind of recovery can be either due to the elimination of etoricoxib by embryonic metabolism, or it could be due to the generation of new COX-2 protein. In any case, such an increase in COX-1 activity combined with a measurable decrease of COX-2 activity was shown for the first time in any tissue. In contrast to our findings with chick embryos, earlier studies with mice showed functional compensation by COX-2 activity for COX-1, but not vice versa [22,23]. Research suggests that PGs do not interfere in compensatory mechanisms of COX isozymes in-vitro in the mouse lung fibroblasts [24]. They also confirmed the positive regulation of COX-2 by PGE₂ and PGF_{2α} in the same system, which could be a plausible mechanism of action for the reactivation of COX-2 in treated chick embryos. However, the identification of the key mediator molecules for heightened COX-1 activity needs further experimentation. In an effort to extend our study to identify the functional compensation of COX-2 by COX-1, we measured the levels of their downstream effectors – the prostanoids.

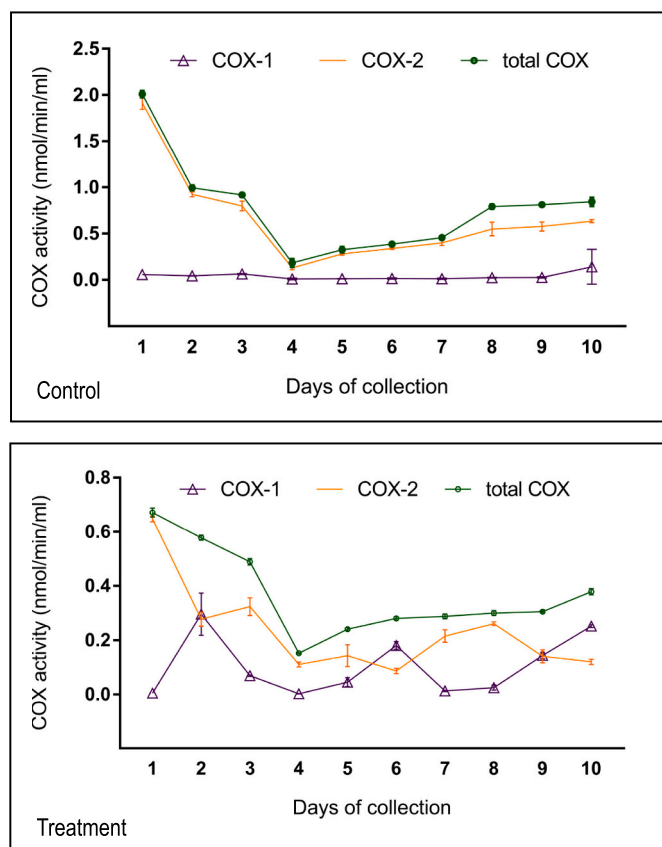


Fig. 5. Activity of COX in day 1 to 10 chick embryos. The upper panel shows control group COX activity, the lower panel shows treatment group COX activity, $n = 6$.

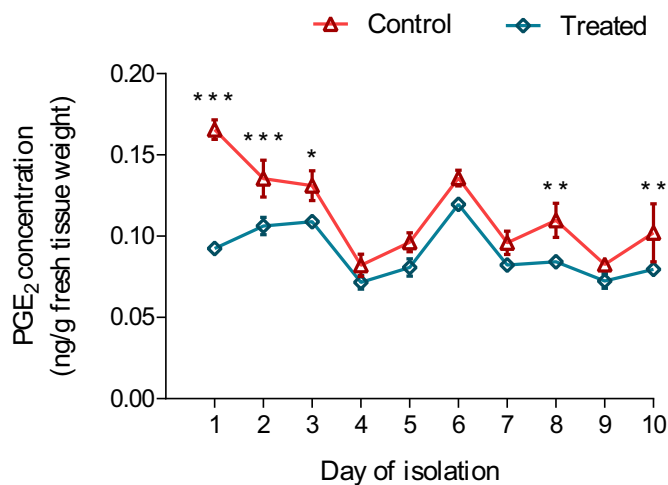


Fig. 6. Mean concentration of PGE₂ in day 1 to 10 chick embryos. * $p \leq 0.05$, ** $p \leq 0.01$, *** $p \leq 0.001$, $n = 3$.

We performed a concomitant analysis of four major prostanoids – PGD₂, PGE₂, PGF_{2 α} , and TXA₂, whose biosynthesis is initiated by both COX-1 and COX-2. TXA₂ is short-lived in most tissues, and so its level was deciphered using the more stable isoform TXB₂ [25]. The only prostanoid to decrease in the etoricoxib treated group as compared to control group was PGE₂ in this study. This significant drop in the level of PGE₂ may have aroused by an isoform-specific regulation pattern for the isomerases, downstream of the COX enzymes. Alternately, it could be

Table 2

Concentration of Prostanoids in the control and etoricoxib treated chick embryos. Values are expressed as Mean \pm SEM *** $p \leq 0.001$, $n = 30$ for each of the two groups.

Analyte	Concentration (ng/g fresh tissue weight)	
	Control	Treatment
PGF _{2α}	03.06 \pm 0.525	02.86 \pm 0.107
TXB ₂	08.73 \pm 0.229	08.51 \pm 1.453
PGD ₂	18.13 \pm 1.162	17.97 \pm 2.998
PGE ₂	04.74 \pm 0.257	02.00 \pm 0.608***

due to differential regulation of the tissue-specific prostanoid synthases. COX-2, for instance, is known to be functionally coupled to one of the downstream isomerases mPGES-1 [26]. Therefore, changes in COX-2 activities could affect the levels of PGE₂ more than those of other prostanoids. Diaz-Munoz et al. (2010) observed that macrophages challenged with bacterial lipopolysaccharide (LPS) showed heightened PGE₂ production due to the concerted synthesis of these two coupled enzymes [27]. Moreover, the LPS challenge was also shown to result in contrasting regulation of COX-1 and COX-2 isoforms in glial cells of mice as well as in the lungs and hearts of rats [28,29]. Thus, in our system, wherein the PGE₂ concentration may be largely COX-2-derived, and increased COX-1 activity cannot compensate for this loss, the remaining prostanoids seem to remain unaffected after specific COX-2 inhibition. Notably, the maintained trend of PGE₂ hike at day-6 in treatment group (Fig. 6) suggests that COX-1 might be playing a role in such increase. This hike also corresponds to the elevated COX-1 activity at the same timepoint (Fig. 5).

Interestingly, PGE₂ is suspected as a teratogen if present at abnormal concentrations since the 1970s [30]. However, earlier studies only revealed its concentration-dependent mortality data in chick embryos [30]. The current study throws more light on this idea by suggesting novel roles of PGE₂ in organogenesis. On the other hand, Etoricoxib-like NSAIDs are increasingly used across the globe to reduce pain. However, their usage during the conception period by women has been found to result in an increased risk of miscarriage [31]. Our findings, which demonstrate the induction of serious morphological defects with NSAID-treated chick embryos along with the concomitant perturbations to PGE₂ levels, suggest a possible reason for these epidemiological observations in humans. Given that the maintenance of prostanoids in the crucial narrow concentration range during the embryogenesis of chicks is critical to proper embryo development, our findings certainly suggest that more detailed studies should be undertaken to assess the risks of NSAID consumption in pregnant women or those women actively wishing to conceive.

CRediT authorship contribution statement

Urja Verma: Data curation. **Maheswor Gautam:** Investigation. **Bhaval Parmar:** Data curation, Writing – original draft. **Kashmira Khaire:** Writing – review & editing. **David S. Wishart:** Writing – review & editing. **Suresh Balakrishnan:** Conceptualization, Methodology, Writing – review & editing.

Declaration of competing interest

The authors declare that they have no known competing financial interests or personal relationships that could have appeared to influence the work reported in this paper.

The authors declare no conflict of interest. COX-2 is both, constitutive and inducible during embryogenesis.

Acknowledgements

This work was supported by the Department of Biotechnology, New

Delhi (Grant No. BT/PR11467/MED/31/270/2014). UV is thankful to The Maharaja Sayajirao University of Baroda for providing fellowship and The Metabolomics Innovation Centre, University of Alberta, for the training of LC-MS/MS, and travel grant under the 'Research Hotel' program.

Appendix A. Supplementary data

Supplementary data to this article can be found online at <https://doi.org/10.1016/j.bbalip.2021.158889>.

References

- [1] D.L. Simmons, R.M. Botting, T. Hla, Cyclooxygenase isozymes: the biology of prostaglandin synthesis and inhibition, *Pharmacol. Rev.* 56 (2004) 387–437.
- [2] C.D. Loftin, D.B. Trivedi, H.F. Tian, et al., Failure of ductus arteriosus closure and remodeling in neonatal mice deficient in cyclooxygenase-1 and cyclooxygenase-2, *PNAS.* 98 (2001) 1059–1064.
- [3] B. Liu, L. Qu, S. Yan, Cyclooxygenase-2 promotes tumor growth and suppresses tumor immunity, *Cancer Cell Int.* 15 (2015) 106.
- [4] N. Hashemi Goradel, M. Najafi, E. Salehi, B. Farhood, K. Mortezaee, Cyclooxygenase-2 in cancer: a review, *J. Cell. Physiol.* 234 (2019) 5683–5699.
- [5] P.R. Buch, I. Ranadive, I. Desai, S. Balakrishnan, Cyclooxygenase-2 interacts with MMP and FGF pathways to promote epimorphic regeneration in lizard *Hemidactylus flaviviridis*, *Growth Factors* 36 (2018) 69–77.
- [6] P.R. Buch, I. Desai, S. Balakrishnan, COX-2 activity and expression pattern during regenerative wound healing of tail in lizard *Hemidactylus flaviviridis*, *Prostaglandins & Other Lipid Mediat.* 135 (2018) 11–15.
- [7] J.E. Dinchuk, B.D. Car, R.J. Focht, et al., Renal abnormalities and an altered inflammatory response in mice lacking cyclooxygenase II, *Nature* 378 (1995) 406–409.
- [8] H. Lim, B.C. Paria, S.K. Das, et al., Multiple female reproductive failures in cyclooxygenase 2-deficient mice, *Cell* 91 (1997) 197–208.
- [9] S. Sen Roy, P.B. Seshagiri, Expression and function of cyclooxygenase-2 is necessary for hamster blastocyst hatching, *Mol. Hum. Reprod.* 19 (2013) 838–851.
- [10] M. Shim, J. Foley, C. Anna, Y. Mishina, T. Eling, Embryonic expression of cyclooxygenase-2 causes malformations in axial skeleton, *J. Biol. Chem.* 285 (2010) 16206–16217.
- [11] K.M. Stanfield, R.R. Bell, A.R. Lisowski, M.L. English, S.S. Saldeen, K.N.M. Khan, Expression of cyclooxygenase-2 in embryonic and fetal tissues during organogenesis and late pregnancy, *Birth Defects Res.* 67 (2003) 54–58.
- [12] B.D. Janković, K. Isaković, M.L. Lukić, N.L. Vujanović, S. Petrović, B.M. Marković, Immunological capacity of the chicken embryo. I. Relationship between the maturation of lymphoid tissues and the occurrence of cell-mediated immunity in the developing chicken embryo, *Immunology* 29 (1975) 497.
- [13] R. Parsad, Some statistical techniques for bio-efficacy trials 16 (2010) 62–76.
- [14] S.C. Chapman, J. Collignon, G.C. Schoenwolf, A. Lumsden, Improved method for chick whole-embryo culture using a filter paper carrier, *Dev. Dyn.* 220 (2001) 284–289.
- [15] K.J. Livak, T.D. Schmittgen, Analysis of relative gene expression data using real-time quantitative PCR and the 2⁻ΔΔCT method, *Methods* 25 (2001) 402–408.
- [16] M.M. Bradford, A rapid and sensitive method for the quantitation of microgram quantities of protein utilising the principle of protein-dye binding, *Anal. Biochem.* 72 (1976) 248–254.
- [17] V. Urja, K. Khaire, S. Balakrishnan, G.K. Uggini, Chick embryonic cells as a source for generating in vitro model of muscle cell dystrophy, *In Vitro Cell. Dev. Biol. Anim.* 54 (2018) 756–769.
- [18] Y.J. Kang, U.R. Mbye, C.J. DeLong, M. Wada, W.L. Smith, Regulation of intracellular cyclooxygenase levels by gene transcription and protein degradation, *Prog. Lipid Res.* 46 (2007) 108–125.
- [19] M.Z. Zhang, J.L. Wang, H.F. Cheng, R.C. Harris, J.A. McKenna, Cyclooxygenase-2 in rat nephron development, *Am. J. Physiol. Ren. Physiol.* 273 (1997) F994–F1002.
- [20] F.G. Smith, A.W. Wade, M.L. Lewis, W. Qi, Cyclooxygenase (COX) inhibitors and the newborn kidney, *Pharmaceuticals* 5 (2012) 1160–1176.
- [21] C. Rheinlaender, S.C. Weber, N. Sarioglu, E. Strauß, M. Obladen, P. Koehne, Changing expression of cyclooxygenases and prostaglandin receptor EP4 during development of the human ductus arteriosus, *Pediatr. Res.* 60 (2006) 270–275.
- [22] J. Reese, N. Brown, B.C. Paria, J. Morrow, S.K. Dey, COX-2 compensation in the uterus of COX-1 deficient mice during the pre-implantation period, *Mol. Cell. Endocrinol.* 150 (1999) 23–31.
- [23] X. Li, L.L. Ballantyne, M.C. Crawford, G.A. FitzGerald, C.D. Funk, Isoform-specific compensation of cyclooxygenase (Ptgs) genes during implantation and late-stage pregnancy, *Sci. Rep.* 8 (2018) 1–13.
- [24] V. Vichai, C. Suyarnesthakorn, D. Pittayakhajonwut, K. Sriklung, K. Kirtikara, Positive feedback regulation of COX-2 expression by prostaglandin metabolites, *Inflamm. Res.* 54 (2005) 163–172.
- [25] A. Benigni, C. Chiabrando, A. Piccinelli, et al., Increased urinary excretion of thromboxane B2 and 2, 3-dinor-TxB2 in cyclosporin A nephrotoxicity, *Kidney Int.* 34 (1988) 164–174.
- [26] B. Samuelsson, R. Morgenstern, P.J. Jakobsson, Membrane prostaglandin E synthase-1: a novel therapeutic target, *Pharmacol. Rev.* 59 (2007) 207–224.
- [27] M.D. Díaz-Muñoz, I.C. Osma-García, C. Cacheiro-Llaguno, M. Fresno, M.A. Íñiguez, Coordinated up-regulation of cyclooxygenase-2 and microsomal prostaglandin E synthase 1 transcription by nuclear factor kappa B and early growth response-1 in macrophages, *Cell. Signal.* 22 (2010) 1427–1436.
- [28] S.F. Liu, R. Newton, T.W. Evans, P.J. Barnes, Differential regulation of cyclooxygenase-1 and cyclo-oxygenase-2 gene expression by lipopolysaccharide treatment in vivo in the rat, *Clin. Sci.* 90 (1996) 301–306.
- [29] M. Font-Nieves, M.G. Sans-Fons, R. Gorina, et al., Induction of COX-2 enzyme and down-regulation of COX-1 expression by lipopolysaccharide (LPS) control prostaglandin E2 production in astrocytes, *J. Biol. Chem.* 287 (2012) 6454–6468.
- [30] T.V.N. Persaud, R.A. Mann, K.L. Moore, Teratological studies with prostaglandin E2 in chick embryos, *Prostaglandins* 4 (1973) 343–350.
- [31] D.K. Li, J.R. Ferber, R. Odouli, C. Quesenberry, Use of nonsteroidal anti-inflammatory drugs during pregnancy and the risk of miscarriage, *Am. J. Obstet. Gynecol.* 219 (2018) 275–e1.

18TH NATIONAL RESEARCH SCHOLAR'S MEET

BY THE STUDENTS, FOR THE STUDENTS



Gratefully acknowledges

Bhaval Parmar

For participation in Oral Presentation

Held on 8th and 9th December, 2022 at
Advanced Centre for Treatment, Research and Education in Cancer (ACTREC),
Tata Memorial Centre (TMC), Navi Mumbai, India.

Dr. Sudeep Gupta
Director,
ACTREC

Dr. Navin Khattry
Dy. Director,
CRC-ACTREC

Dr. Prasanna Venkatraman
Dy. Director,
CRC-ACTREC

Vaishnavee Chikhale
Organising Secretary,
NRSM



**International Conference on
Breakthroughs in Toxicology and Human Health (ICBTHH)
and
39th Annual Meeting of Society of Toxicology**



December 27-29, 2019

Jiwaji University, Gwalior-474011, India
School of Studies in Zoology and Biochemistry

CERTIFICATE

This is to certify that Prof./Dr./Mr./Ms./.....*Bhawal Parmar*..... chaired the
from *Maharaja Sayajirao University, Baroda*..... session/ delivered an invited talk/attended/presented a research paper/poster on the topic entitled
Etacicoxib.....*domestic hen*.....

and actively participated in the deliberations during the conference.

Nalini Srivastava
Prof. Nalini Srivastava
Convener

Y.K. Jaiswal
Prof. Y.K. Jaiswal
Organising Chair

Alok Dhawan
Prof. Alok Dhawan
President STOX, India

Sangeeta Shukla
Prof. Sangeeta Shukla
Vice Chancellor